Chem. Rev. **1988**, *88*, 31–53

Molybdenum Oxide Bronzes with Quasi-Low-Dimensional Properties

MARTHA GREENBLATT

Chemistry Department, Rutgers, The State University of New Jersey, New Brunswick, New Jersey 08903

Received April 28, 1987 (Revised Manuscript Received August 3, 1987)

Contents

Martha Greenblatt received her Bachelor's degree from Brooklyn College in Brooklyn, New York, in 1962, and her Ph.D. from the Polytechnic Institute of Brooklyn in 1967. At the Polytechnic Institute of Brooklyn she worked with Professor E. Banks, and after completion of her degree, she stayed on at the Institute as Assistant Professor of Chemistry for a few years. She was a Visiting Scientist at the Weizmann Institute in 1972/1973. She joined the faculty of Rutgers University in July 1974, where she is presently Professor of Chemistry. She spent the summer of 1980 as Visiting Professor at the Clarendon Laboratory, Oxford University, England, and a sabbatical year at Bell Laboratories, Murray Hill, NJ, in 1980/1981. Her research interests are in the area of solid-state chemistry, including the synthesis and characterization of quasi-low-dimensional transition-metal compounds, fast ionic motion in solids, and, more recently, high-temperature superconducting materials.

I. Introduction

The term bronze, originally coined for Na_xWO_3 compounds by Wohler in 1825,[1] is now applied to a variety of crystalline phases of the transition metal oxides; these are usually ternary compounds of the type $A_xM_zO_y$ with intense color and metallic luster, metallic or semiconducting properties, and resistance to attack by nonoxidizing acids, but binary oxides with similar properties also qualify. Ternary bronzes have been prepared in which M is Ti, V, Mn, Nb, Ta, Mo, W, or Re and A is H, NH_4^+, or an alkali, alkaline earth, rare earth, group 11, group 12, or other metal ion.

The alkali metal tungsten bronzes, A_xWO_3, have been studied most intensively and have been reviewed in the past.[2–5] Extensive reviews including all bronze phases studied were presented by Banks and Wold[3] and Hagenmuller[5] nearly 20 years ago. A brief review of the molybdenum bronzes (results up to ca. 1980) was given more recently in a chapter on lower valence molybdenum oxides.[6] A recent review of transition metal oxides with quasi-low-dimensional properties updates some of these results.[7]

Interest in all types of transition metal oxide bronzes has continued in recent years. A computer search of “tungsten bronzes” and “vanadium bronzes” in *Chemical Abstracts* came up with 670 and 331 references, respectively, since 1967. However, in the past 5 years most of the interest has focused on the study of molybdenum bronzes and especially on the so-called “blue bronzes” $A_{0.3}MoO_3$ (A = K, Rb, Tl). This interest is primarily concerned with structural and physical properties, unique to some of these bronzes, which include highly anisotropic transport properties characteristic of quasi-one-dimensional and quasi-two-dimensional (quasi-1D and quasi-2D) metallic systems, the metal-to-semiconductor transition driven by a charge density wave (CDW) state, and superconductivity. Nonohmic behavior of the conductivity with increasing dc electric field above a small threshold potential (E_T) and a collection of related phenomena previously associated with a moving of “sliding” CDW in the chalcogenides $NbSe_3$,[8] TaS_3,[9] and $(TaSe_4)_2I$[10] have also been observed in these structurally different classes of oxide materials and are intensely studied in several laboratories worldwide.[11] These new findings on the nonlinear transport and related properties of $K_{0.3}MoO_3$ and $Rb_{0.3}MoO_3$ have been recently reviewed in several articles[12] and chapters in a series of books written on

0009-2665/88/0788-0031$06.50/0

quasi-low-dimensional materials.[7,12a]

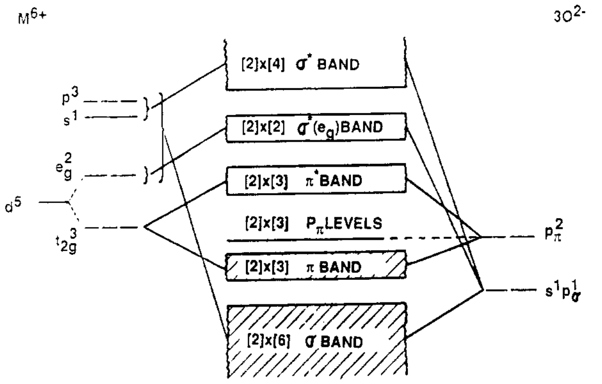

Figure 1. Schematic band structure applicable to the bronzes above the Peierls transition (after ref 52).

Molybdenum bronzes may be classified on the basis of similarity of color, stoichiometry, and structure as the blue bronzes, $A_{0.3}MoO_3$ with A = K, Rb, and Tl; the red bronzes, $A_{0.33}MoO_3$ with A = Li, K, Rb, Cs, and Tl; and the purple bronzes, $A_{0.9}Mo_6O_{17}$ with A = Li, Na, K, and Tl. The most recently prepared rare-earth molybdenum bronzes, $A_{0.08}MoO_3$ (A = La, Ce, Eu, Gd, Lu), appear to form yet another new class in this system.[13] $Cs_{0.19}MoO_3$, a blue bronze, is unique both in stoichiometry and in structure.

In contrast to the W bronzes, which have simple three-dimensional (3D) structures of corner-sharing WO_6 octahedra with the A cations located in cubooctahedral cavities, the Mo bronzes have complex, layered-type structures with edge- and corner-sharing MoO_6 octahedra forming infinite two-dimensional sheets which are held together by A cations (with the exception of $Li_{0.33}MoO_3$ and $Li_{0.9}Mo_6O_{17}$ as will be discussed later). While the W bronzes A_xWO_3 are nonstoichiometric ($0 < x \leq 1$), these Mo bronzes are stoichiometric or very nearly so.

The bronzes $Na_{0.90-0.97}MoO_3$, $K_{0.89-0.93}MoO_3$, $K_{0.5}MoO_3$, and $Rb_{0.27}MoO_3$, which are prepared by high-pressure synthesis and are isostructural with their W bronze analogues, have not been studied extensively, but are known to be metallic.[3,5] A relatively new class of compounds are the hydrogen molybdenum bronzes H_xMoO_3 ($0 < x \leq 2.0$), in which the hydrogen is topotactically inserted into the MoO_3 matrix to yield four unique phases: $H_{0.23-0.40}MoO_3$, blue, orthorhombic; $H_{0.85-1.04}MoO_3$, blue, monoclinic; $H_{1.55-1.72}MoO_3$, red, monoclinic; and H_2MoO_3, green, monoclinic. The structure of each is closely related to that of the structure of the MoO_3 host, and the properties vary with H content.[6] This article will review primarily the ternary molybdenum bronzes, although some new results on related binary and ternary molybdenum oxides, which are not strictly conventional bronzes but exhibit similar quasi-low-dimensional behavior, will also be discussed.

II. Preparation

The first molybdenum bronzes, $K_{0.3}MoO_3$, $K_{0.33}MoO_3$, and $Na_{0.9}Mo_6O_{17}$, were prepared by Wold et al.[14] by electrolytic reduction of A_2MoO_4–MoO_3 melts[14] under carefully controlled conditions of temperature and composition. This technique has been used in slight variations to produce a variety of alkali metal molybdenum bronzes,[15-27] $Tl_{0.3}MoO_3$,[28] and $A_{0.08}MoO_3$ with A = La, Ce, Eu, Gd, and Lu[13] in single-crystal form. Most of the crystals grown in this way are usually plateletlike, elongated along one of the crystal axes, and typically 5 × 2 × 1 mm^3 in size. The crystals can be cleaved easily parallel to the platelet plane.

Polycrystalline samples of a variety of alkali metal bronzes have been prepared from stoichiometric mixtures of A_2MoO_4, MoO_3, and MoO_2 in evacuated sealed gold tubes at various temperatures;[29-31] all of the known Mo bronzes may be prepared similarly in polycrystalline form in evacuated quartz tubes at the appropriate temperature for each.[32-38]

More recently, a temperature gradient flux technique has been developed for the growth of good-quality single-crystal molybdenum bronzes from a stoichiometric mixture of reactants according to the equation $nA_2MoO_4 + 2(1 - n)MoO_3 + nMoO_2 \rightarrow 2A_nMoO_3$.[32-38] In a typical experiment the reactant mixture is pelletized and sealed in an evacuated quartz tube which is placed in a two-zone furnace. The charge end of the ampule is placed in the hot zone and a temperature gradient is maintained across the length of the tube by setting the cool end of the furnace ~50 °C lower than the hot zone. For compositions $0.2 \leq n \leq 0.5$, melting of the charge throughout the tube is facilitated by appropriate adjustment of the temperature of the two zones. Single-crystal bronzes grow in the melt; different types of bronzes may grow at different regions of temperature in the same ampule. The type of bronze and the quality of the crystals in each case are highly dependent on the value of n and on the temperature gradient of the furnace. Optimal conditions of these parameters have been determined for the growth of large, good-quality single crystals of most of the common ternary molybdenum bronzes.[32-38] Large single crystals of the binary phases of the Mo_4O_{11} and MoO_2 oxides can also be obtained by the temperature gradient flux technique.

The alkali metal molybdenum bronzes, isostructural with known tungsten bronzes, have been prepared by high-pressure reaction between either alkali metal molybdate, MoO_3, and Mo metal powder[39] or alkali metal azide and MoO_3[40] at 65-kbar pressure and 770–1270 K. These phases have been reviewed in detail before[3,5,6] and will not be discussed here.

Chemical or electrochemical reduction of MoO_3 in acidic media was shown to yield a series of solid phases H_xMoO_3 ($0 < x \leq 2.0$).[41-51] Deuteriated molybdenum bronzes, D_xMoO_3, have also been prepared for various values of x.[47,48]

III. Band Structure

Figure 1 shows a schematic diagram of the band structure developed by Goodenough[52] for ReO_3 and first applied to the molybdenum bronzes by Dickens and Neild.[53] It is assumed that the local octahedral coordination of the metal atom by six oxygen atoms largely determines the common bonding pattern in the bronzes (A_xMO_3) and the parent oxide (e.g., MoO_3, WO_3, and ReO_3). For a discrete MO_6 unit (in the 4d transition metal series) 5p, 5s, and 4d(e_g) orbitals overlap with six sp hybrid orbitals of the oxygen atom to give a set of six bonding σ and six antibonding σ* molecular orbitals. In the extended lattice, the discrete energy levels arising from this structure unit will broaden into bands. The metal 4d(t_{2g}) orbitals can overlap with three of the surrounding oxygen pπ orbitals per octahedron to form bonding π and antibonding π^* bands. The σ and π bands are filled and constitute the valence bands separated by a large energy gap (3–4 eV) from the π^* conduction band. This band is empty in WO_3 and MoO_3, so these materials are insulators, but is partially filled in ReO_3, which is a metal. In the bronzes $A_xM_yO_z$, the A cations transfer their valence electrons to the usually empty π^* levels with strong d character. The extent of delocalization of the d electrons characterizes the transport and optical properties of any specific bronze. The orbitals of the A cation do not contribute to the formation of these levels as confirmed by several experiments.[54,55]

In the vanadium bronzes, $A_xV_2O_5$, the 3d electrons are mostly localized, and these compounds are semiconductors, although some of the β-$A_xV_2O_5$ phases show quasi-1D metallic behavior. In contrast, the 5d electrons of the tungsten bronzes, A_xWO_3, are delocalized because of the greater radial extension of the 5d orbitals,[56] and these compounds are metals at all temperatures. In the molybdenum bronzes the 4d orbitals have a radial extension intermediate between the 3d (localized) and 5d (delocalized) states, and these materials show complex electronic behavior; the blue ($A_{0.3}MoO_3$) and purple ($A_{0.9}Mo_6O_{17}$) bronzes are metallic at ambient temperature, but exhibit a metal-to-semiconductor and a metal-to-metal transition, respectively, while the red bronzes ($A_{0.33}MoO_3$) are semiconducting. Interestingly, the $A_{0.08}MoO_3$ rare-earth bronzes also exhibit semiconducting character, even though the composition roughly corresponds to one-third of the alkali metals in the $A_{0.3}MoO_3$ phases.[13] However, the structural properties of the rare-earth bronzes are yet to be determined. Recent band calculations using a tight-binding band scheme by Whangbo et al. on both the blue[57] and purple bronzes[58] are consistent with the schematic band structure in Figure 1, but provide greater detail as will be shown later.

IV. The Blue Bronzes ($A_{0.3}MoO_3$)

A. Crystal Structure

The structure of $K_{0.3}MoO_3$ was first solved by Graham and Wadsley.[59] More recent single-crystal X-ray diffraction structural refinement of $K_{0.3}MoO_3$, $Rb_{0.3}MoO_3$,[60] and $Tl_{0.3}MoO_3$[28] shows that all of these blue bronzes are isostructural and form with monoclinic symmetry, in space group $C2/m$ with 20 molecules per unit cell, in an arrangement essentially as originally determined by Graham and Wadsley. The structure is built of infinite sheets of distorted MoO_6 octahedra held together with the A cations as shown in Figure 2a. The MoO_6 layers consist of clusters of ten edge-sharing octahedra linked by corners in the [010] and [102] directions (Figure 2b). Another view of the structure as infinite chains of MoO_6 octahedra sharing corners along the monoclinic b direction is illustrated in Figure 2a. Of the three crystallographically unique Mo sites per cluster only two of them, Mo(2) and Mo(3),[28,60] are involved in these infinite chains. Moreover, it has been established by bond length–bond strength considerations[61] that over 80% of the 4d electron density is found on the Mo(2) and Mo(3) sites[28,59] in the chains along the b axis.

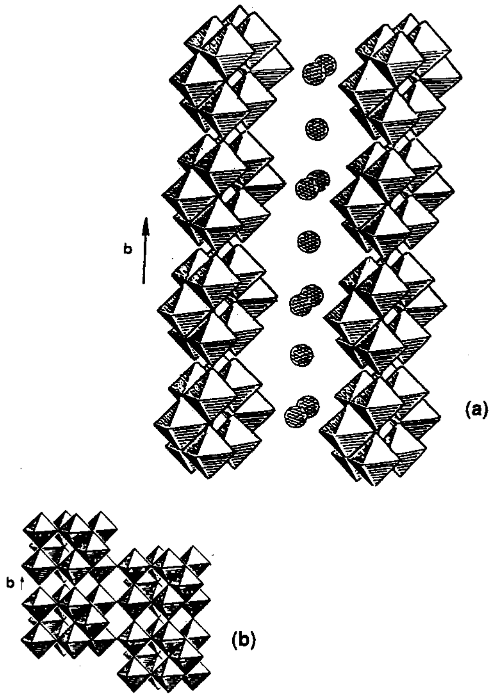

Figure 2. (a) Crystal structure of the $A_{0.3}MoO_3$ blue bronzes showing infinite chains of Mo(2)– and Mo(3)–oxygen octahedra parallel to b. (b) Infinite layers of MoO_6 octahedra made up by corner sharing of the basic ten-cluster MoO_6 edge/corner-sharing octahedra along the b and [102] directions (after ref 12a).

TABLE 1. Unit Cell Parameters of $A_{0.3}MoO_3$ Bronze Phases

	$K_{0.30}MoO_3$[a]	$Tl_{0.30}MoO_3$[b]	$Rb_{0.30}MoO_3$[a]
unit cell	monoclinic	monoclinic	monoclinic
space group	$C2/m$	$C2/m$	$C2/m$
a, Å	18.2587 (7)	18.486 (1) (18.543 (3))	18.6354 (3)
b, Å	7.5502 (4)	7.5474 (6) (7.567 (4))	7.555 (1)
c, Å	9.8614 (4)	10.0347 (7) (10.067 (2))	10.094 (2)
β, deg	117.661 (4)	118.377 (6) (118.39 (2))	118.842 (5)

[a] The values given in ref 64 have been transformed to a $C2/m$ unit cell. [b] Reference 34; the values in parentheses are given by ref 28. The small differences between the two values may reflect small deviations in Tl stoichiometry or other concentrations of lattice or impurity defects.

Unit cell parameters of the known $A_{0.3}MoO_3$ phases are given in Table 1. The data show significant variations in a, c, and β with A ion; however, the unique monoclinic b axis remains practically unchanged with increasing effective size of the A cation. This suggests that the chainlike coupling of corner-sharing MoO_6 octahedra along the b axis is independent of the nature of the A ion in the blue bronzes. Since the stoichiometry corresponds exactly to the formula $A_{0.3}MoO_3$ ($A_3Mo_{10}O_{30}$), all crystallographic sites are occupied and therefore no crystallographic disorder is expected. In the next section it will be shown how the low-dimensional electronic, magnetic, and optical properties are accounted for by the structure.

B. Physical Properties: The Peierls Transition

Wold et al.[14] and Bouchard et al.[15] were first to study the electrical properties of unoriented samples of

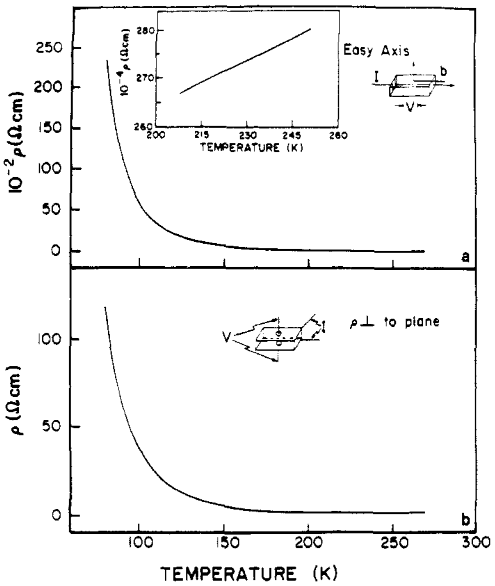

Figure 3. Temperature variation of the resistivity of $Tl_{0.3}MoO_3$: (a) current and voltage in the plane of the platelet crystals parallel to the *b* axis; (b) current and voltage perpendicular to *b* and the (201) cleavage plane. Inset shows detail of decreasing resistivity with decreasing temperature in the range ~250–200 K.

$K_{0.3}MoO_3$ about 20 years ago and established the existence of a metal-to-semiconductor transition at ~180 K. Later, it was shown by Perloff et al.[16] that the electrical conductivity is highly anisotropic. Fogle and Perlstein[62] proposed several models to account for the metal-to-semiconductor transition, including the Mott–Hubbard model[63] with a short-range electron–hole attraction and an excitonic–insulator model[64] for the semiconductor state. They also noted that for $K_3Mo_{10}O_{30}$ with three electrons per lattice point, a new Brillouin zone could form at the Fermi surface (E_F) by a doubling of the periodicity due to a small distortion of the $Mo_{10}O_{30}$ clusters, which could also lead to the observed metal-to-semiconductor transition. However, they failed to find a lattice distortion by X-ray diffraction.[16,65] In addition, they reported nonohmic behavior of conductivity at low temperature above a critical voltage, although the source of that behavior then was not recognized.

More recently, Brusetti et al.[21] reexamined the conductivity, thermopower, and magnetic properties of $K_{0.3}MoO_3$ and have shown that the resistivity of $K_{0.3}MoO_3$ is about an order of magnitude larger along [102] in the plane of the layers than along *b*, and even higher along the [$\bar{2}$01] direction perpendicular to the layers of MoO_6 octahedra. Similar anisotropy of the temperature variation of ρ is found for $Rb_{0.3}MoO_3$ and $Tl_{0.3}MoO_3$, which is illustrated for the latter in Figure 3.[12,25,28,34]

The optical reflectivity data obtained by Travaglini et al.[66] for $K_{0.3}MoO_3$ and Jandl et al. for $Rb_{0.3}MoO_3$[67] established that above 180 K these bronzes are truly quasi-1D metals. At 300 K, the blue bronzes show a metallic behavior with a plasma edge for light polarized along *b*, and semiconducting type behavior with an absorption edge of light polarized along [102]. The plasma frequency, ω_p = 2.7 eV, along *b* corresponds to a carrier concentration resulting from a complete charge transfer of the valence s electrons of the alkali metal into the π^* conduction band (Figure 1). $\omega_p \ll 0.03$ eV along [102] indicates that the carrier concentration in the semiconducting direction is 4–5 orders of magnitude less than in the metallic direction.[66] These results are in excellent agreement with the structural data discussed above which show that >80% of the 4d electrons are on Mo sites involved in infinite chains of corner-sharing MoO_6 octahedra parallel to the *b* axis of the *monoclinic unit cell. In terms of the schematic* band structure (Figure 1), the 4d electrons are delocalized in the π^* conduction band which forms primarily by the overlap of Mo(2) and Mo(3) $4d(t_{2g})$ and oxygen $p(\pi)$ orbitals. Thus while the *bonding* is clearly 3D in the blue bronzes, the transport and optical properties are quasi-1D, because the distribution of unpaired electrons is very anisotropic.

In the semiconducting state, the gap was found to be 0.15 eV. However, the resistivity does not follow a simple activated behavior below the transition temperature (T < 180 K), except in the narrow temperature interval 30 < T < 70 K, where the activation energy E_a ~ 0.03 eV.[16,21] Below 30–20 K the crystals are highly resistive ($\sigma \approx 10^{-14}$ $(\Omega\ cm)^{-1}$) and show nonlinear (nonohmic) behavior of conductivity for very small values of dc current.[62] The low-temperature conductivity is not intrinsic and is associated with defects of impurity levels in the gap. Electron spin resonance (ESR) studies corroborate the presence of Mo^{5+} ($4d^1$) localized states at low temperature;[68] these and similar states may well be responsible for the transport properties below 100 K.

The thermopower is highly anisotropic above 180 K in the plane of the layers, consistent with 1D character; it does not follow $1/T$ behavior below 180 K down to 38 K, supporting the extrinsic nature of conductivity in the semiconducting state.[16,69] The Hall coefficient is positive above 180 K and changes sign at the transition,[15,69] indicating that at least two bands (one electron and one hole) are involved in transport. Raman scattering studies[70–72] show the appearance of a line at ~50 cm^{-1} in the semiconducting phase which has an anomalous temperature dependence below 180 K, suggesting that it is related to the CDW state. A specific heat anomaly, found in $K_{0.3}MoO_3$ and $Rb_{0.3}MoO_3$ between about 150 and 190 K, is additional evidence of the CDW-driven phase transition.[73]

The idea that the electronic energy of a 1D metal could be lowered by a charge density wave (CDW) was first predicted by Peierls[74] and Fröhlich.[75] In 1D conductors a coupled instability of the conduction electrons and phonons at $2k_F$ (where k_F is the Fermi wave vector or reciprocal unit cell dimension of the 1D metal) at low temperature leads to a modulation of the charge density coupled to a lattice distortion of a CDW state which is accompanied by an opening of a gap at the Fermi surface as shown in Figure 4. The states near the gap below the Fermi energy (E_F), which are pushed down in energy, are occupied, while those that are raised are empty; the total electronic energy is therefore lowered. If the decrease in electronic energy is greater than the potential energy cost of the lattice distortion, a charge density wave will spontaneously appear. Subsequent work has shown that this instability is not restricted to one-dimensional systems. In the past 15 years CDW has been experimentally verified in a number of quasi-low-dimensional organic and inorganic compounds, including $NbSe_3$, TaS_2, $TaSe_2$, $(NbSe_4)_{3.33}I$, and (Ta-

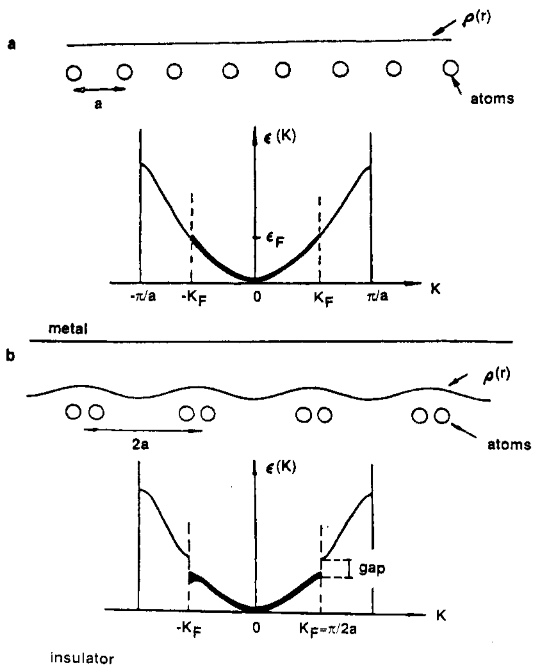

Figure 4. Peierls distortion in a one-dimensional metal with a half-filled band (after ref 76): (a) undistorted metal; (b) Peierls insulator with period doubling.

$Se_4)_2I$, and is fairly well understood in the transition metal di- and trichalcogenides.[76,77]

A chemically and structurally different class of compounds, the blue bronzes, are new examples of materials which exhibit a CDW-driven metal-to-semiconductor transition. Although a CDW-driven phase transition generally results in anomalies in the temperature variation of the resistivity, magnetic susceptibility, and specific heat, unambiguous evidence of the CDW state is the observation of superlattice lines by electron, X-ray, or neutron diffraction which confirm the modulation of the lattice sites. X-ray diffuse scattering studies by Pouget et al.[25] have shown conclusively that the transition at 180 K in the blue bronzes is a Peierls transition leading to an incommensurate semiconducting CDW state. When the wave vector, Q, of the distortion is commensurate with the lattice, the distortion of the charge and atomic displacement simply gives the crystal a larger unit cell. Specifically, if $Q = a^*/3$ (where $a^* = K/a$; $K = 1$ or some other constant) then the unit cell dimension a is 3 times the old unit cell dimension and the crystal is periodic. When Q is incommensurate, no unit cell can contain the exact period of both the wave and the underlying crystal lattice. The crystal is no longer periodic; the whole sample is the unit cell. In $K_{0.3}MoO_3$ and $Rb_{0.3}MoO_3$ ($Tl_{0.3}MoO_3$ has not yet been studied by diffraction techniques below the transition) even at room temperature diffuse streaks normal to the b^* direction are observed which condense into well-defined superlattice reflections below 180 K.[25] The satellite reflections are located at $\pm(1 - q_b)b^*$ ($b^* = K/b$) from the main reflections, where q_b, the component of Q along b, is 0.26 ± 0.01 at 110 K.[25]

Analysis of the X-ray data shows that motion of the Mo(2)–O_6 and Mo(3)–O_6 octahedra is mainly involved in the structural distortion and that the alkali metals are not significantly affected. Similar X-ray diffraction studies by Sato et al.[78] of the superlattice reflections of the blue bronzes confirmed these findings. The temperature dependence of the Q vector studied by various investigators[79-81] indicates that $1 - q_b$ is incommensurate with decreasing temperature and approaches a commensurate value of 0.75 near 100 K. According to Fleming et al.[80] a true lock-in incommensurate-to-commensurate transition occurs near 100 K. This is consistent with the data of Pouget et al.[81] and with recent ^{87}Rb NMR data of $Rb_{0.3}MoO_3$ which show a narrowing of the NMR line around 90 K corresponding to a finite number of sites with substantial hysteresis.[82] However, the existence and the nature of the incommensurate–commensurate transition near 100 K remain controversial; recent NMR results seem to incidate that the system remains incommensurate down to the lowest temperatures.[73,83] Careful heat capacity measurements of $Rb_{0.3}MoO_3$ between 50 and 150 K show a kink at 100 K, but there is no conclusive evidence of a phase transition.[84]

The thermal variation of the satellite intensity follows approximately the Bardeen–Cooper–Schrieffer (BCS) law predicted by mean field theory.[85-87] However, the ratio of the Peierls gap 2Δ to the Peierls temperature kT_P is found to be $\sim$8, compared to $\sim$3.5 predicted by the simple mean field theory.

Pouget et al.[86] have shown that the wave vector of the Peierls distortion along the chain direction is $2k_F = {}^3/_4b^*$. If there is complete charge transfer from the A metal to the conduction band, there will be 3 conduction electrons per $A_3Mo_{10}O_{30}$. The k_F value is consistent with either a doubly degenerate conduction band or two one-dimensional bands overlapping at the Fermi surface. Recent tight-binding band calculations on an $Mo_{10}O_{30}$ slab of the blue bronze structure by Whangbo and Schneemeyer are consistent[57] with two overlapping d-block bands roughly three-fourths filled as shown by Figure 5a. The upper and lower Fermi surfaces of the first band (Figure 5b) are found to be nested (Figure 5d) to the lower and upper Fermi surfaces of the second band (Figure 5c), respectively, by an identical wave vector $1 - q_b = 0.75b^*$. This explains why there is a single CDW in the blue bronze, as proposed by Pouget et al.[86] The band calculations also predict a third d band which lies only 0.012 eV above the Fermi level.[57] Thus thermal excitation of electrons from the two conduction bands into the bottom of the third band will decrease the $1 - q_b$ value of the latter bands. This accounts for the temperature dependence of $1 - q_b$, which increases gradually from $\sim 0.72b^*$ at room temperature to $\sim 0.75b^*$ below T_c.

More recently, an X-ray photoemission spectroscopy (XPS) study of $K_{0.3}MoO_3$ showed a conduction band extending 2 eV below the Fermi level with largely Mo 4d character,[88] corroborating the band calculation.[57] Angular-resolved UV photoemission studies measured at 300 K on $K_{0.3}MoO_3$ crystals establish that $0.27 < k_F < 0.36$ Å^{-1}.[89] This is in excellent agreement with the value obtained from the position of the X-ray satellite reflections in the low-temperature CDW phase ($2k_F = 0.75b^*$, $k_F = 0.312$ Å^{-1}). This direct measurement of k_F corroborates the model of $2k_F$ instability responsible for the phase transition at 180 K, and this may be the first example where this is so clearly established.

The magnetic susceptibility, χ, of $K_{0.3}MoO_3$ has been measured by several investigators[15,21,24,26,68,90] and is

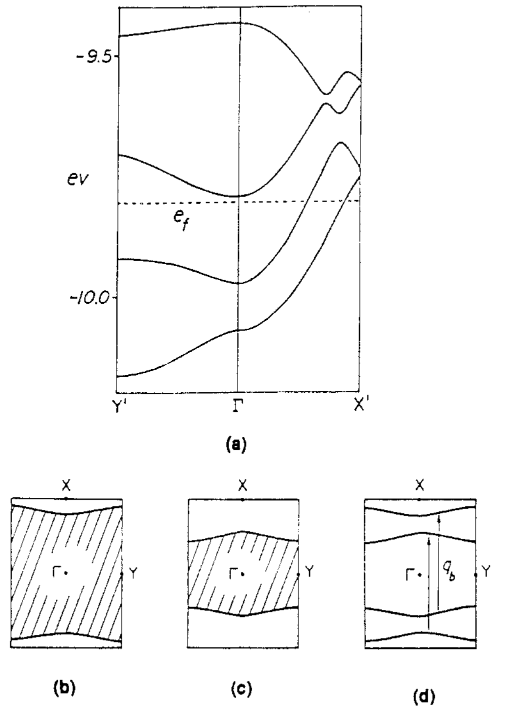

Figure 5. (a) The bottom four d-block bands calculated for a real $Mo_{10}O_{30}$ slab of $K_{0.3}MoO_3$ along $\Gamma \rightarrow X'$ and $\Gamma \rightarrow Y'$ (approximately along the b and [102] directions). The dashed line refers to the Fermi level. (b,c) The Fermi surfaces associated with two partially filled d-block bands of a real $Mo_{10}O_{30}$ slab, where the wave vectors of the shaded and unshaded regions lead to occupied and unoccupied band levels, respectively. (d) Nesting of the Fermi surfaces of the first and second band. (a–d after ref 57.)

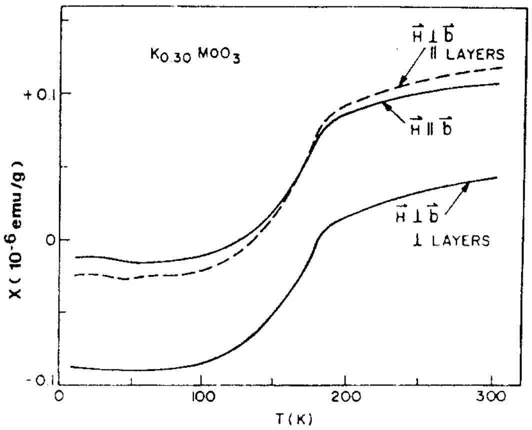

Figure 6. Temperature variation of the magnetic susceptibility of $K_{0.3}MoO_3$ as a function of temperature for different orientations of the magnetic field (after ref 24).

found to be highly anisotropic as shown in Figure 6. In most metals, χ is temperature independent. The observed susceptibility is the result of several contributions: $\chi = \chi_{dia} + \chi_{Pauli} + \chi_{Van\,Vleck}$. The anisotropy of χ is attributed to the Van Vleck paramagnetism due to the anisotropy of the band structure. The weak temperature dependence of χ in $K_{0.3}MoO_3$ between ~180 K and room temperature is consistent with fluctuations into the Peierls state as expected in a one-dimensional system. This temperature dependence can be ascribed to a pseudogap of 200 K above 180 K.[90] The zero temperature Peierls gap is ~1200 K, which is in fairly good agreement with the value obtained by optical studies.[91] The decrease in the magnetic susceptibility from ~180 K is due to the opening of a gap at the Fermi surface associated with the CDW transition and to the vanishing of Pauli contribution. A small anomaly of unknown origin is observed near 50 K, which was also seen in the susceptibility of $Tl_{0.3}MoO_3$.[34]

The similarities of the structural and transport properties of $K_{0.3}MoO_3$, $Rb_{0.3}MoO_3$, and $Tl_{0.3}MoO_3$ suggest that a similar mechanism of transport is operative in all three systems. The nearly identical T_c values close to 180 K in each indicate that the electronic properties are determined primarily by the MoO_6 octahedral network, which is nearly the same in each bronze as evidenced by the almost identical values of the crystallographic b dimension (Table 1).

The effect of various substitutional impurities on the electrical properties of the blue bronzes has been investigated. Substitution of nonisoelectronic vanadium in $K_{0.3}Mo_{1-x}V_xO_3$ with $x = 0.04$ stabilizes the semiconducting state, and no transition is found in the resistivity.[21] It is possible that the smaller V^{5+} (0.46 Å) ions substituting for Mo^{6+} (0.59 Å) produce some structural distortion which stabilizes the semiconducting phase. Alternatively, the V ions may interfere with the overlap of Mo t_{2g} and O $p\pi$ orbitals and induce localization. The substitution of Rb for K even in large concentrations (50 atom %) does not modify the physical properties strongly as expected, since the properties of the K and Rb blue bronzes are very similar and the alkali metal does not participate in the band structure.[26] In contrast, substitution of isoelectronic W for Mo has a dramatic effect and decreases the transition temperature sharply even at low doping levels of W ($K_{0.3}Mo_{1-x}W_xO_3$ with $x = 0.004$); the metallic-type behavior vanishes at $x = 0.03$ W content at room temperature and below,[26] again indicating that disorder in the Mo chain induces localization. ^{57}Fe Mössbauer studies of Fe substituted for Mo in $K_{0.3}MoO_3$ also give evidence of local distortions taking place at the Peierls transition.[84] Iron ions appear to substitute for the alkali metal ions and act as impurity traps pinning the CDW.[89]

A recent study of cesium substitution indicates that a large concentration of Cs (~50 atom %) in $(Rb_{1-x}Cs_x)_{0.3}MoO_3$ yields the blue bronze with an order of magnitude increase in the conductivity and a small shift in the metal-to-semiconductor transition to lower temperature; this is somewhat surprising, since the Cs analogue of $A_{0.3}MoO_3$ does not appear to form.[92]

C. Moving Charge Density Waves

Fröhlich first suggested motion of an incommensurate CDW as leading to enhanced conductivity.[75] Nonlinear conductivity attributed to the sliding of CDW was first reported for $NbSe_3$ in 1976 by Monceau et al.[89] Since then, a considerable amount of work has been devoted to the study of moving CDW's and associated phenomena in NbS_3 and, additionally, in TaS_3, $(TaSe_4)_2I$, and the blue bronzes.[11,12]

Dumas et al. were the first to establish that $K_{0.3}MoO_3$ shows nonlinear transport due to the sliding of CDW.[93] Since the discovery of nonlinear transport, the blue bronzes have been studied extensively.[11,12,27,91,94] There are four important phenomena associated with the moving CDW which have been characterized.

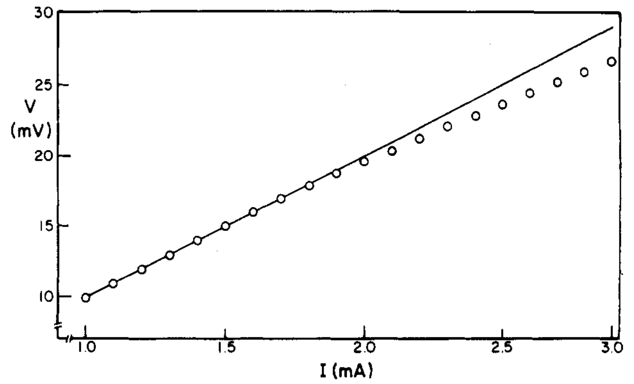

Figure 7. Current–voltage characteristics of $Tl_{0.3}MoO_3$ at liquid N_2 temperature.

1. Nonlinear dc Conductivity

Figure 7 shows the current–voltage (*I–V*) characteristics of $Tl_{0.3}MoO_3$ at $T = 77$ K. Current is proportional to voltage (ohmic behavior) below a threshold field, E_T, ~300 mV/cm for this sample and typically 10–200 mV/cm (very *small* electric fields). In the ohmic regime, the phase of the CDW is "pinned" to the lattice either by impurities and defects or by commensurability. Above E_T, the CDW is "depinned", begins to move in the applied field, and contributes the additional conductivity, resulting in a nonlinear (nonohmic) current–voltage response.

The threshold field has been studied as a function of the concentration of defects created either by electron irradiation or by doping. E_T is found to increase linearly with concentration of defects introduced by electron bombardment.[95] A similar, linear dependence of E_T with increasing amounts of W substitution into Mo sites in $K_{0.3}MoO_3$ is observed. A linear increase of E_T with impurity or defect concentration is attributed to strong pinning centers; the CDW phase is determined by a single impurity atom. Rb impurities substituted for K provide so-called weak pinning centers;[26] E_T increases as the square of the impurity concentration. In this case the CDW phase is averaged over an array of impurities.

2. ac Response to a dc Bias

Additional evidence for CDW motion is provided by the time-dependent voltage response to a dc current bias. Known also as "noise", this takes the form of a broad-band response and a discrete frequency response (narrow-band noise) for applied dc electric fields above E_T; the latter is illustrated for a sample of $K_{0.3}MoO_3$ in Figure 8. Narrow-band noise has been difficult to observe in bronze crystals. The noise spectrum consists of one fundamental frequency, F_1, the so-called "washboard" frequency and its harmonics. While the origin of the narrow-band noise remains controversial,[96a] it is associated with an absorption by the CDW at a frequency corresponding to the CDW velocity (the "washboard frequency"). Putting it another way, the effect is due to the interaction of the CDW phase distribution with the impurity potential, or washboard, arising from the distribution of defects and impurities in the sample.

Another manifestation of noise is the observation of transient voltage oscillations to a current step response of $K_{0.3}MoO_3$.[96b] These oscillations result from enhanced damping of the CDW at a frequency which is equal to the narrow-band noise frequency even though steady-state oscillations are not observed.

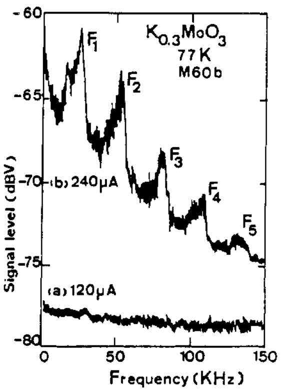

Figure 8. Fourier analysis of the narrow-band noise voltage of $K_{0.3}MoO_3$ at 77 K. Threshold current: $I_t = 130$ μA (after ref 12a).

Current oscillations with very low frequency (in the hertz range) have also been found in the blue bronze.[98] These pulses might be related to the existence of CDW domain boundaries or possible dislocations in the CDW lattice.[12]

3. Enhanced ac Conductivity

Cava et al. have measured the ac conductivity of $K_{0.3}MoO_3$ in the temperature range $60 < T < 101$ K and frequency range 5 Hz to 13 mHz.[97] In the pinned CDW state, the relaxation is that of a single process with a distribution of relaxation times, characteristic of the response of a nonrigid CDW.

At dc biases below E_T the frequency-dependent conductivity can be interpreted in terms of parallel conductivity of "normal" electrons thermally excited above the CDW-induced gap together with relaxation oscillations of the pinned CDW itself.[97] At dc biases above E_T, the response is that of an absorption by the CDW at a frequency corresponding to the CDW velocity (the washboard frequency). The relaxation rate of the CDW decreases with decreasing temperature and apparently goes to zero at low temperatures. The static dielectric constant, ϵ_0, deduced from these data is of the order of 10^7 and follows an Arrhenius-type law. The static dielectric constant, which measures the polarizability of the sample, is enormous.

4. Hysteresis and Memory Effects

In sliding CDW conductors the ohmic and nonlinear responses are functions of the electrical and thermal history of the sample.[99–105] The observed hysteresis is attributed to deformations of the moving CDW. After moving, the pinned CDW never relaxes completely to the ground state; instead it finds a metastable state that depends on the previous history of the sample. A metastable state results in a macroscopic polarization of the sample, and a decay of this polarization may be infinitely long.

Experimentally, metastability of the CDW response was first seen by Gill in $NbSe_3$. Gill measured the sample resistance following a bias pulse large enough to depin the CDW.[99] He observed that whenever the sign of a pulse was reversed, the sample conductivity at the leading edge of the pulse was initially higher than the steady-state value as shown in Figure 9. This

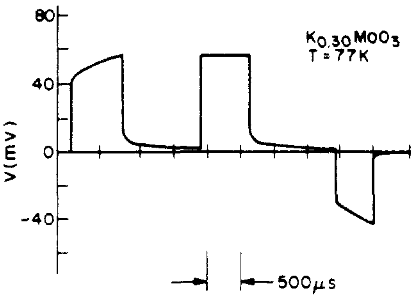

Figure 9. Response of $K_{0.3}MoO_3$ to a repetitive series of constant-current pulses consisting of two positive pulses followed by one negative pulse. All pulses are in excess of threshold (after ref 102).

manifestation of metastability is now known as the "pulse sign memory effect". The conductivity decay occurs on time scales of several hundred microseconds in $K_{0.3}MoO_3$.[102] This is because the CDW phase, which is distorted upon the application of a pulse, remains in a high elastic energy metastable state after the pulse. If the next pulse is in the opposite direction, the CDW cannot start moving immediately. Instead it must first distort in the opposite sense by progressing through a hierarchy of metastable states.

Experimentally, metastability also has other manifestations.[102-105] It has been shown that metastable states result in transient changes in the moving state and long-term changes in the properties of pinned CDW. Thermally stimulated depolarization (TSD) experiments show that a metastable CDW state is characterized by a frozen dipole moment.[106] When the CDW has been frozen into a metastable state by cooling to 4.2 K in the presence of small electric fields, $K_{0.3}MoO_3$ acts as a current source on heating. As the sample is warmed and the induced dipoles thermally relax, the image charges flow through the external circuit, producing currents as large as 10^{-9} A in $K_{0.3}MoO_3$. This implies enormous polarizations, confirming the dielectric results. The current emitted is dependent on the magnitude of the field applied on cooling, reflecting differences in the frozen-in metastable states. The relaxation of the CDW from its metastable state is thermally activated and occurs with a distribution of relaxation times. X-ray scattering experiments on $K_{0.3}MoO_3$ show that there is a metastable, field-induced loss of crystalline order in field-cooled specimens.[107-109] For temperatures below 100 K, the relaxation time from metastable states exceeds hours. The disorder is characterized by local motion of the CDW rather than a microscopic loss of long-range order. This loss of order is in the transverse direction (i.e., between the infinite chains of Mo octahedra) according to the X-ray results.

The unifying feature of these measurements is that the nonlinear CDW response is dominated by a large number of degrees of freedom. CDW transport is best viewed as motion of a deformable medium, rather than the sliding of a rigid object.

V. The Purple Bronzes ($A_{0.9}Mo_6O_{17}$)

A. Crystal Structure

The first purple molybdenum bronze, $Na_{0.9}Mo_6O_{17}$, was prepared more than 20 years ago by Wold et al. by fused-salt electrolysis.[14] The crystal structure of this bronze was partly solved by Stephenson on a twinned crystal, who reported an "average" distorted perovskite-type structure.[110] Reau et al. have prepared polycrystalline specimens of $A_{0.9}Mo_6O_{17}$ with A = Li, Na, and K and reported all three compounds to be isostructural, pseudohexagonal, monoclinic phases.[30] Gatehouse et al. prepared untwinned single crystals of the Li, Na, and K purple bronzes and attempted to solve the structure of each by X-ray analysis.[111,112] They solved the structure of the Na and K phases based on centered monoclinic symmetry; however, they were unable to solve the structure of the Li compound, which they reported to have primitive monoclinic symmetry.[112]

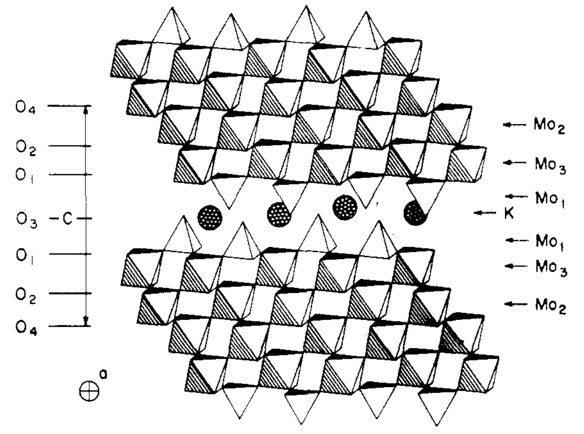

Figure 10. Idealized structure of $K_{0.9}Mo_6O_{17}$ viewed along the *a* axis showing the infinite layers of corner-sharing molybdenum–oxyggen polyhedra stacked along *c* and held together by K ions located in icosahedral sites (after ref 27).

A more recent redetermination[113] of the crystal structure of $K_{0.9}Mo_6O_{17}$, shown in Figure 10, is in essential agreement with that reported by Gatehouse et al.[86] The crystal structure is trigonal with space group $P\bar{3}$. The ideal structure of hexagonal $K_{0.9}Mo_6O_{17}$ can be described in terms of slabs of Mo–O corner-sharing polyhedra. Each slab of Mo–O polyhedra consists of four layers of ReO_3-like MoO_6 octahedra sharing corners which are terminated on either side by a layer of MoO_4 tetrahedra which share corners with adjacent MoO_6 octahedra. These slabs are perpendicular to the *c* axis and are separated from each other by a layer of potassium ions in a KO_{12} icosahedral enrivonment of oxygens. The MoO_4 tetrahedra in adjacent layers do not share corners, so that the Mo–O–Mo bonding, infinite in the *a* and *b* directions, is disrupted in the c direction. The effective Mo valences are +6 on the Mo (Mo(1) of Figure 10) in tetrahedral sites and +5.1 and +5.8 on the two crystallographically nonequivalent Mo in octahedral sites (Mo(2) and Mo(3), respectively, in Figure 10). Thus the 4d electrons of molybdenum atoms are located in the two-dimensional slabs of octahedra and the structural properties are expected to lead to a very anisotropic Fermi surface which is consistent with the observed quasi-2D conductivity.[22] The structure is very similar to the monoclinic form of Mo_4O_{11}.[114]

Recently, the structure of $Li_{0.9}Mo_6O_{17}$ has been solved by Onoda et al.[115] In Figure 11 the crystal structure projected in the *ac* plane shows significant differences from that of the $K_{0.9}Mo_6O_{17}$ structure (Figure 10). There are six crystallographically unique molybdenum ions in the unit cell; Mo(3) and Mo(6) are tetrahedrally coordinated while the other molybdenums occupy oc-

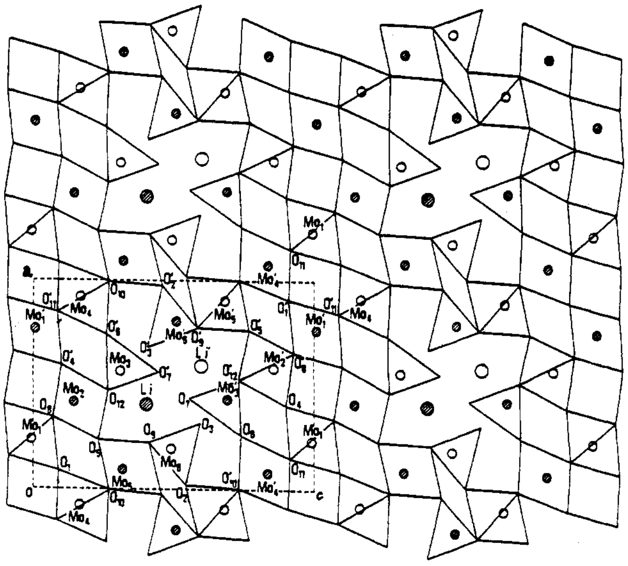

Figure 11. Crystal structure of $Li_{0.9}Mo_6O_{17}$ projected in the *ac* plane. Open and hatched circles indicate atomic positions at $y = {}^1/_4$ and ${}^3/_4$, respectiely (after ref 115).

tahedral sites. Chains of four MoO_6 octahedra corner share along the [102] direction, and ReO_3-like slabs are formed by three of the corner-sharing MoO_6 octahedra. The slabs are interconnected by corner-sharing octahedra and tetrahedra (Figure 11) along the *c* direction. Thus, unlike in the $K_{0.9}Mo_6O_{17}$ structure, the Mo–O–Mo interactions along the *c* direction are uninterrupted. However, the Mo–O–Mo network has a much higher degree of cross-linking in the *ab* plane than parallel to *c*, so a quasi-low-dimensional character is maintained. The Li^+ ions occupy large nine-oxygen-coordinated cavities created by the 3D molybdenum polyhedral network structure. The effective Mo valences are 5.05, 5.72, 5.76, 5.01, 5.76, and 5.76 for Mo(1), Mo(2), Mo(3), Mo(4), Mo(5), and Mo(6), respectively. Thus in contrast to $K_{0.9}Mo_6O_{17}$ all the molybdenums have appreciable conduction electrons. Nevertheless, most of the electrons are located on Mo(1) and Mo(4) octahedral sites, which are associated in pairs to form –Mo(1)–O(11)–Mo(4)–O(11)– double-zigzag chains, extending along the *b* axis. The Mo ions involved in MoO_4 and MoO_6 polyhedra interconnecting the slabs each have a valence of 5.76 and fewer unpaired electrons. Therefore the structural properties should lead to highly anisotropic electronic transport.

The crystal structure of $Na_{0.9}Mo_6O_{17}$ has been redetermined very recently;[116] the monoclinic space group of *C*2 symmetry as previously suggested by Gatehouse et al.[111,112] has been confirmed. The structure of the Na compound is essentially identical with that of the $K_{0.9}Mo_6O_{17}$ phase.[116]

Recently, single crystals of the thallium analogue of the purple bronzes, $TlMo_6O_{17}$, have been prepared by the gradient flux technique.[35] On the basis of a single-crystal X-ray determination of the unit cell parameters, this phase appeared to be isostructural with the K compound.[35] This has been confirmed by a recent structural investigation,[117] which shows that although the space group of $TlMo_6O_{17}$ is $P\bar{3}m1$, different from that of $K_{0.9}Mo_6O_{17}$, which is $P\bar{3}$, the structural differences are very small and affect only two of the oxygen positions. Furthermore, the A site is fully occupied only in the thallium bronze.[117]

TABLE 2. Unit Cell Parameters of $A_{0.9}Mo_6O_{17}$ Phases

	$Li_{0.9}Mo_6O_{17}$[a]	$Na_{0.9}Mo_6O_{17}$[b]	$K_{0.9}Mo_6O_{17}$[c]	$TlMo_6O_{17}$[d]
unit cell	monoclinic	monoclinic	trigonal	trigonal
space group	$P2_1/m$	*C*2	$P\bar{3}$	$P\bar{3}m1$
a, Å	9.499 (1) (9.487)	9.591 (2) (9.565)	5.538 (1)	5.543 (2) (5.557 (3))
b, Å	5.523 (1) (5.519)	5.518 (1) (5.525)	5.538 (1)	5.543 (2) (5.557 (3))
c, Å	12.762 (2) (12.748)	12.983 (2) (12.978)	13.656 (2)	14.000 (2) (14.030 (4))
β, deg	90.61 (1) (90.59)	89.94 (1) (90.09)		

[a] Reference 115; values in parentheses are from NDPPA data.[119] [b] Reference 116; in parentheses are values for a $Na_{0.88}Mo_6O_{17}$ composition obtained by least-squares refinement of powder data.[33] [c] Reference 113. [d] Reference 35; values given in parentheses are from ref 117.

In Table 2 crystallographic parameters of the $A_{0.9}Mo_6O_{17}$ phases are summarized. The compounds in Table 2 are listed in order of increasing effective ionic radii for A^+ in a 12-coordinated oxygen polyhedra.[118] When the monoclinic cell parameters of the Li and Na phases are approximated to a pseudohexagonal cell with $a_{hex} \simeq b$ and $c_{hex} \simeq c$ for easier comparison with $K_{0.9}Mo_6O_{17}$ and $TlMo_6O_{17}$, it is seen that a_{hex} is practically unchanged with increasing effective size of the A cations. This indicates that the 2D network structure of the Mo_6O_{17} infinite slabs is independent of the nature of the A cation (except, of course, in the case of the Li purple bronze, where the polyhedral Mo network is significantly different; however, even in the Li compound the Mo–O–Mo interactions in the slabs along *b* are very similar to those in the other purple bronzes). In contrast, c_{hex} increases dramatically with increasing ionic size of A^+ in the bronze. Despite the similarity of the effective ionic radii of Tl^+ (1.70 Å) and Rb^+ (1.72 Å), efforts in our group to synthesize the Rb analogue have not been successful so far.

It appears that $TlMo_6O_{17}$, like $K_{0.9}Mo_6O_{17}$, has a fixed composition, unlike $Na_{0.9}Mo_6O_{17}$, which has a small range of nonstoichiometry in Na ($0.84 \leq Na \leq 0.96$).[30,33,35] However, while in $TlMo_6O_{17}$ all the alkali metal sites are fully occupied, in the Na and K phases these sites are about 0.1 mol^{-1} vacant.

B. Charge Density Wave Instabilities

The results of four probe resistivity measurements for $Li_{0.9}Mo_6O_{17}$, $Na_{0.9}Mo_6O_{17}$, $K_{0.9}Mo_6O_{17}$, and $TlMo_6O_{17}$ single crystals are shown in Figures 12, 13, 14, and 15, respectively.[22,35,120,121] The resistivity is strongly anisotropic and orders of magnitude higher along the *c* axis than in the plane perpendicular to *c*, where it is nearly isotropic in each case, except for $Li_{0.9}Mo_6O_{17}$ for which a large anisotropy is present in the *ac* plane. The purple molybdenum oxide bronzes are quasi-2D metals and exhibit a metal-to-metal transition (T_c) at low temperature. However, the transition temperature at the transport anomaly varies over a wide range, depending on the nature of the alkali metal ion, in contrast to the blue bronzes, for which the metal-to-semiconductor transition (T_{ms}) is ~180 K for each of the reported three phases ($A_{0.3}MoO_3$, A = K, Rb, Tl). A change in the sign of the temperature dependence of the resistivity is found at approximately 24, 80, 120, and 113 K for the lithium, sodium, potassium, and thallium purple bronzes, respectively. Furthermore, while the

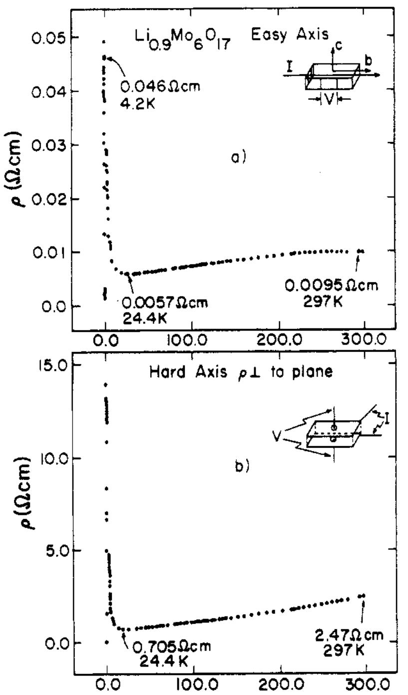

Figure 12. Temperature variation of the resistivity of $Li_{0.9}Mo_6O_{17}$ from 0.3 to 300 K: (a) current in the plane of the platelet crystal; (b) current perpendicular to the plane of the platelet parallel with *c*.

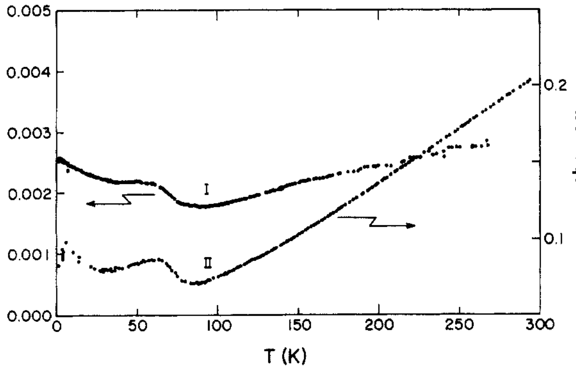

Figure 13. Temperature variation of the resistivity of $Na_{0.9}Mo_6O_{17}$ from 15 to 300 K: (I) current in the plane of the platelet crystal; (II) current perpendicular to the plane of the platelet parallel with *c*.

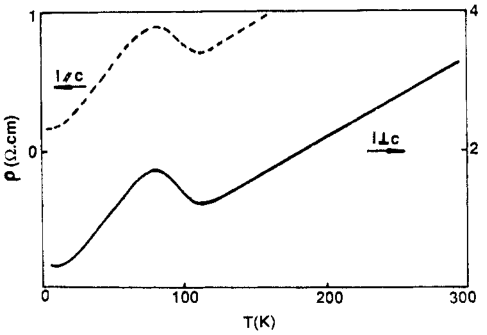

Figure 14. $K_{0.9}Mo_6O_{17}$: resistivity vs temperature measured with the current along and perpendicular to the *c* axis (after ref 22).

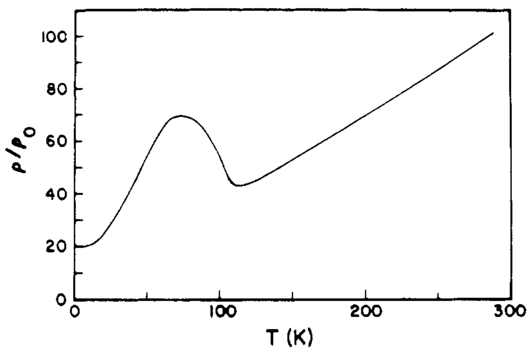

Figure 15. Temperature variation of the resistivity of $TlMo_6O_{17}$.

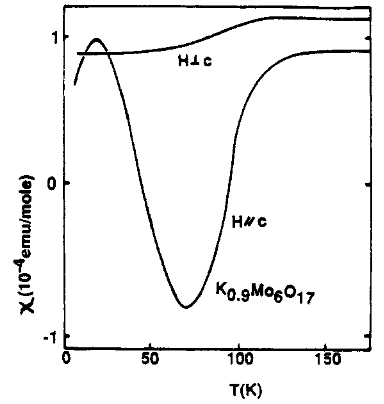

Figure 16. Temperature variation of the susceptibility of $K_{0.9}Mo_6O_{17}$ measured with the magnetic field parallel or perpendicular to the *c* axis (after ref 124).

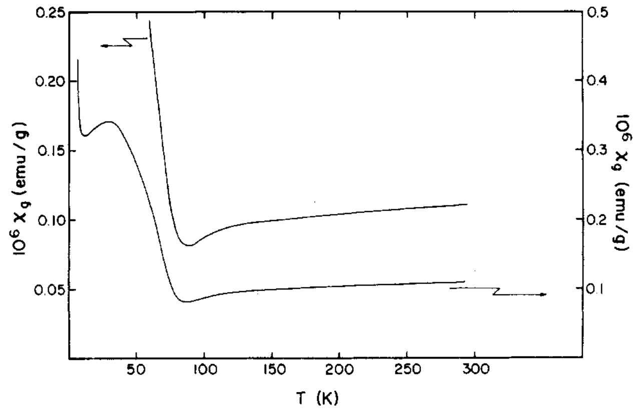

Figure 17. Temperature variation of the magnetic susceptibility of $Na_{0.9}Mo_6O_{17}$.

resistivities of the Na, K, and Tl compounds show a sigmoidal-shaped transition similar to that found in the quasi-1D compound $NbSe_3$,[8] the lithium phase shows a sharp increase (about an order of magnitude) in the resistivity at ~24 K and a transition to a superconducting state at $T_c \simeq 1.9$ K.[121-123] This suggests that the electronic properties of the purple bronzes are somehow affected by the nature of the alkali metal ion, probably by subtle structural variations of the respective compounds. The significantly different transport behavior of the Li compound is consistent with the structural properties of the Li compound, which were shown to be substantially different from those of the Na, K, and Tl analogues.

The temperature variation of magnetic susceptibility, χ, of $Li_{0.9}Mo_6O_{17}$ shows Pauli paramagnetic behavior and no anisotropy down to 4 K.[121,123] In $K_{0.9}Mo_6O_{17}$ the susceptibility exhibits a large anisotropy similar to the behavior seen in the resistivity and a sharp decrease in the susceptibility at ~120 K corresponding to the onset of the anomaly in the resistivity (Figure 16). At $T <$ 70 K the susceptibility increases and another transition

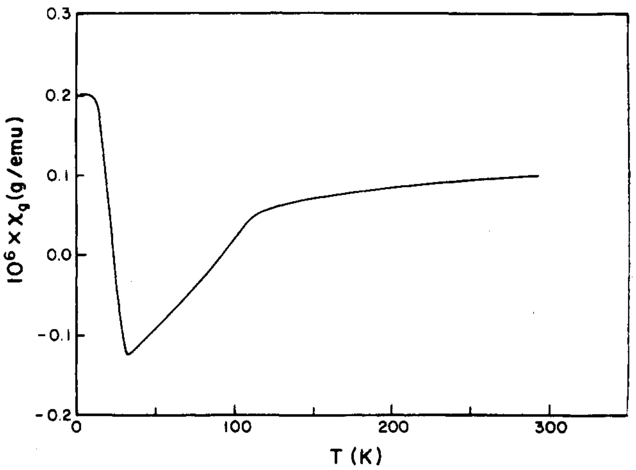

Figure 18. Temperature dependence of the magnetic susceptibility of $TlMo_6O_{17}$.

is evident in the vicinity of 30 K.[124] The origin of this last transition is unknown; it has been suggested that it may be related to the onset of a spin density wave (SDW).[125] The sodium purple bronze shows similar complex behavior (Figure 17): there appears to be a small drop in the susceptibility near ~80 K, where ρ begins to increase, a definite transition at $T < 100$ K, and another transition at $T \sim 40$ K similar to the 30 K transition observed in the K compound. The temperature dependence of the susceptibility of the thallium purple bronze (Figure 18) shows a transition at 110 K, which is also seen in the resistivity; the transition near ~30 K is not observed in the resistivity (Figure 15).[35,117]

As was discussed above, the structure of $A_{0.9}Mo_6O_{17}$ bronzes with A = Na, K, and Tl consists of layers of corner-sharing MoO_6 octahedra and MoO_4 tetrahedra that make up the Mo_6O_{17} slabs, which are connected by the alkali metal ions. The 4d electrons are delocalized primarily on the octahedral molybdenums in the 2D *ab* planes, which are well separated along the *c* direction. This gives rise to the observed quasi-2D metallic behavior. Although the structure of $Li_{0.9}Mo_6O_{17}$ is considerably different from that of the Na, K, and Tl analogues as also reflected in its markedly different electronic transport properties, nevertheless, the quasi-2D (or perhaps quasi-1D) character is maintained.

In quasi-2D metals the Fermi surface may be quasi-cylindrical with respect to an axis perpendicular to the 2D plane and will often show nesting with a wave vector Q parallel to this plane. Such materials are unstable toward lattice distortions of the wave vector Q, which can lead to an opening of a gap at the Fermi surface. This decreases the electronic energy of the system.

In quasi-1D metals the gap opening at the Fermi surface is normally complete, and the Peierls transition is a metal-non-metal transition. In a quasi-2D metal the Peierls-like transition is associated with gap openings only over part of the Fermi surface, and therefore a metal-metal transition is observed. In the $A_{0.9}Mo_6O_{17}$ phases the increase in the resistivity and decrease in the magnetic susceptibility at the metal-metal transition result from the loss of Fermi surface due to formation of gaps associated with the CDW state. Both X-ray diffuse scattering and electron diffraction studies have established that the transition seen in $K_{0.9}Mo_6O_{17}$ and $Na_{0.9}Mo_6O_{17}$ at ~120 and ~80 K, respectively, is due to a CDW instability which leads to a structural transition of a commensurate $2a \times 2a \times c$ state.[126,127] Diffuse scattering seen at room temperature in the single-crystal Weissenberg X-ray photographs of $TlMo_6O_{17}$ may also be an indication of lattice instability.[35] A broad endothermic peak ~120 K in the DSC is further evidence of a structural distortion in this compound.[35]

Assuming that the basic band structure is primarily determined by the Mo–O polyhedra and in view of the similarity of the Mo_6O_{17} network structure of the Na, K, and Tl phases, similar electronic behavior might be expected. We already noted that the onset of the CDW instability varies from 80 K for Na, to 113 K for Tl, to 120 K for K. Although the qualitative shape of the temperature dependence of resistivity at the CDW transition is "sigmoidal" in these three purple bronzes, the temperature variations of the transport properties show significant differences in detail (Figure 12–17). For example, $K_{0.9}Mo_6O_{17}$ is metallic between ~80 and 2 K, but shows an anomaly in χ below ~30 K; in $Na_{0.9}Mo_6O_{17}$ the resistivity is metallic in the range ~ 65–30 K beyond the Peierls-like transition, but ρ increases again below ~30 to 1.5 K. χ vs T indicates even more complex behavior of $Na_{0.9}Mo_6O_{17}$ as discussed above (Figure 17). In $TlMo_6O_{17}$ the resistivity is temperature independent below ~5 K down to ~1.6 K, the limit of temperature measurement. An unambiguous transition to a superconducting state has been observed only in $Li_{0.9}Mo_6O_{17}$ thus far, and nonlinear transport properties attributed to the sliding of the CDW, although sought for, have not been detected in these compounds. The significant differences seen in the transport properties of the $A_{0.9}Mo_6O_{17}$ (A = Na, K, Tl) purple bronzes as a function of the A cation are in contrast to the $A_{0.3}MoO_3$ blue bronzes (A = K, Rb, and Tl) where the transition temperature of the CDW state and general behavior of the transport properties are nearly identical. There is structural evidence that the quasi-2D nature of the $K_{0.9}Mo_6O_{17}$ lattice is maintained in all of these analogues. However, the nature of the A metal ion subtly affects the molybdenum environment and valency in the slabs. This appears to have a considerable effect on the band structure.

The anomalous behavior of $Li_{0.9}Mo_6O_{17}$ compared to that of the Na, K, and Tl analogues has been clarified to some extent by the structural determination. On the basis of the distribution of electrons, which are located primarily on the double chains of Mo(1) and Mo(4) along the *b* axis, the large anisotropy observed in the conductivity is accounted for ($\sigma_b:\sigma_a:\sigma_c \simeq 250:10:1$). The question whether the sharp upturn in the resistivity at 24 K is due to a CDW-driven transition or a localization effect has not been answered unambiguously. Sato and co-workers cite the absence of a decrease in the magnetic susceptibility in the vicinity of 24 K as an argument against the formation of a CDW state[123a] and attribute the resistivity upturn at 24 K to electron localization.[123b] However, similar effects have been observed in the susceptibility of $NbSe_3$ where the CDW onset at 32 K affects only the resistivity.[128] So whether CDW or localization is responsible for the anomaly in the resistivity at 24 K can only be resolved by diffraction experiments below T_c. Matsuda et al. attempted

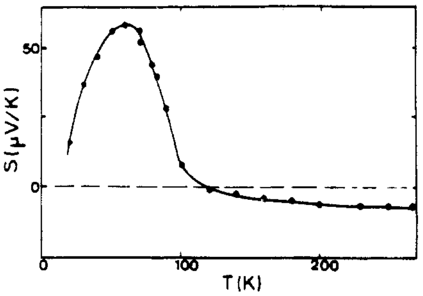

Figure 19. Thermopower vs temperature for $K_{0.9}Mo_6O_{17}$ (after ref 22).

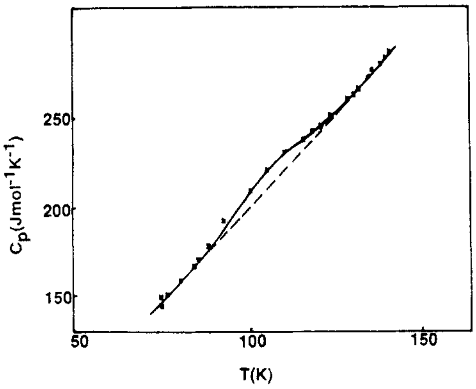

Figure 20. Specific heat (C_p) of a single crystal of $K_{0.9}Mo_6O_{17}$ as a function of temperature (after ref 126).

to find evidence for a competition of CDW and superconductivity in mixed $(Li_{1-x}K_x)_{0.9}Mo_6O_{17}$ and $(Li_{1-x}Na_x)_{0.9}Mo_6O_{17}$ phases, but the transition from superconductivity to CDW behavior is abrupt at $x = 0.48$ and $x = 0.4$, respectively, due to the structural phase transitions.[123a] However, their electron tunneling measurements of a single crystal of $(Li_{0.65}Na_{0.35})_{0.9}Mo_6O_{17}$ show unambiguously that the superconductivity is intrinsic, that the observed energy gap is consistent with the BCS value, and that superconductivity and the sharp resistivity upturn at ~24 K originate from the same electron system in $Li_{0.9}Mo_6O_{17}$.[123c]

The specific heat anomaly found for $Li_{0.9}Mo_6O_{17}$ between 2 and 34 K[27] is in agreement with the transition temperature seen in the resistivity (Figure 12) at ~24 K and shows that a considerable amount of short-range order persists above T_c. Similar specific heat data of $Li_{0.9}Mo_6O_{17}$ down to 1.6 K show a deviation from linearity below T^2 ~ 2.5, which most likely corresponds to the superconducting transition,[27,123] also seen in the resistivity (Figure 12), and which was also confirmed by ac susceptibility measurements at ~2 K.[121,122]

The thermoelectric power (TEP) measured for $K_{0.9}Mo_6O_{17}$ (Figure 19) is small and negative above 120 K, becomes positive at 120 K, and shows a maximum at 70 K.[22] This indicates that at $T > 120$ K the major carriers are electrons while at $T < 120$ K the dominant carriers are holes. This behavior is consistent with a structural transition occurring below 120 K due to the partial opening of a gap at the Fermi surface, which leads to a change in the concentration of both types of charge carriers.

In $K_{0.9}Mo_6O_{17}$ the electrical resistivity (Figure 14), the specific heat (Figure 20),[126] and the intensity of X-ray diffraction superlattice spots (2.5, 2.5, 2) (Figure 21) as a function of temperature strongly suggest that the transition is due to the opening of gaps at the Fermi surface, which start at ~120 K and are fully opened at ~80 K. The satellite intensity is temperature independent at $T < 80$ K. The resistivity decreases as the temperature is further lowered $T < 80$ K, presumably because the gaps begin to close. The electronic energy gained by the distortion of the Fermi surface can no longer compensate the energy needed to distort the lattice as the temperature is lowered.

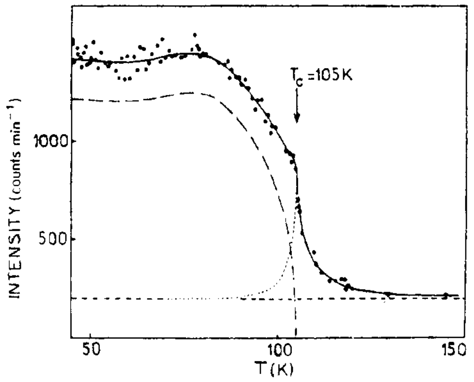

Figure 21. Intensity of the satellite peaks (2.5, 2.5, 2) as a function of temperature (after ref 126). (The horizontal dashed line indicates the background level.)

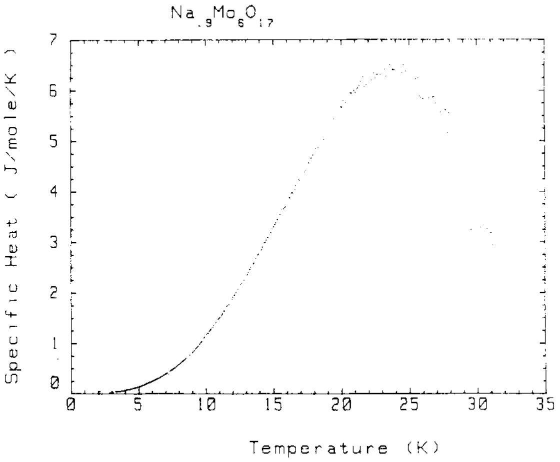

Figure 22. Specific heat (C_p) of $Na_{0.9}Mo_6O_{17}$ as a function of temperature (polycrystalline samples).

The specific heat of $Na_{0.9}Mo_6O_{17}$ in the temperature range 1.5–40 K (Figure 22) shows an anomaly at ~30 K, also seen in the resistivity and susceptibility, which suggests a second transition.[129] The TEP of $TlMo_6O_{17}$ above ~120 K is negative and increases linearly with decreasing temperature as expected for metallic behavior. An anomaly is observed at ~120 K and S increases sharply and becomes positive, indicating that at low temperatures the carriers are mainly holes.[117] The specific heat measured from 300 to 90 K shows a soft maximum at ~117 K, confirming a phase transition near this temperature,[117] which leads to the partial opening of gaps at the Fermi surface suggested by the transport and magnetic properties (Figures 15 and 18).

The thermal data of the purple bronzes are summarized in Table 3. γ, the coefficient of the linear term in the low-temperature heat capacity, is significantly larger for the Li and Na compounds. This may be related to electron correlations and in $Li_{0.9}Mo_6O_{17}$ is consistent with the larger resistivity below T_c. The largest Debye temperature, θ_D, of $Li_{0.9}Mo_6O_{17}$ reflects the increased three-dimensionality as evidenced by the

TABLE 3. Thermal Data for the Purple Bronzes and Molybdenum Oxides Mo_4O_{11}[a]

	T_c, K	ΔS, mJ mol^{-1} K^{-1}	ΔH, J mol^{-1}	γ, mJ mol^{-1} K^{-2}	θ_D, K	ref
$Li_{0.9}Mo_6O_{17}$	24[b]	240	2.6	5	365	27
				6	410	123
$Na_{0.9}Mo_6O_{17}$	80			10	290	27
$K_{0.9}Mo_6O_{17}$	120	530	64	1.6	320	27
				3.9		123
$TlMo_6O_{17}$	120	314 ± 17	36 ± 2			117
	117					35
η-Mo_4O_{11}	109	560	70	3	330	27
	25	37	0.9			
γ-Mo_4O_{11}	100			2.6	410	27

[a] T_c is the onset temperature of the charge density wave transition. γ is the coefficient of the linear term in the low-temperature heat capacity. θ_D is the Debye temperature, ΔH is the enthalpy variation associated with the transition, and ΔS is the entropy of the transition obtained as $\Delta H/T_c$. The accuracy of ΔH and ΔS is limited by the difficulty in estimating the background heat capacity. [b] The exact nature of the resistivity upturn at ~24 K (i.e., whether it is due to a CDW or SDW or localization effect) has not been unambiguously clarified in the Li compound.

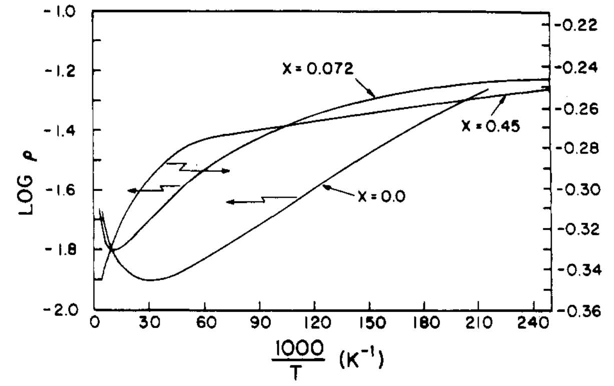

Figure 23. log (resistivity) vs inverse temperature for $Li_{0.9}Mo_{6-x}W_xO_{17}$.

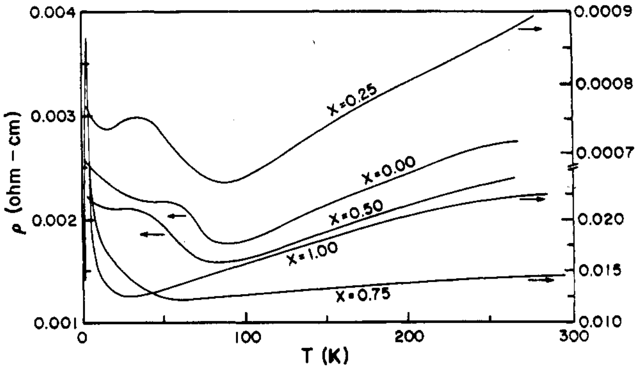

Figure 24. Temperature variation of the resistivity of $(Na_{1-x}Li_x)_{0.9}Mo_6O_{17}$.

3D network structure, and is related to the smaller size of the Li^+ ion and the tighter coordination of Li^+ vs Na^+, K^+, and Tl^+ as indicated by the structural data. At the onset of the CDW instability, T_c increases from Li to K with increasing effective ionic radius of the alkali metal (in 12-coordination); T_c of Tl is anomalously low in terms of the larger effective ionic radius of Tl compared to K. However, in the Tl phase, the alkali metal sites are fully occupied, which may give it the additional stability against the Peierls-like distortion.

Dramatic effects are observed in the electronic properties of tungsten-doped $Li_{0.9}Mo_6O_{17}$.[36,116,123] Even at the lowest W-doping levels (~0.18 atom wt %) the superconducting state near 2 K disappears. A rounding and broadening of the metal–metal transition temperature are seen with increasing tungsten content, which may be attributed to local distortions around the substitutional impurity. In contrast to $K_{0.3}Mo_{1-x}W_xO_3$ in which T_{ms} decreases with increasing W content, in $Li_{0.9}Mo_{6-x}W_xO_{17}$ the transition temperature increases with increasing tungsten content. In addition to the metal–metal transition at ~24 K, another activated conduction state is observed at lower temperature as shown in the log ρ vs $1/T$ plots in Figure 23. This low-temperature anomaly is attributed to impurity defect levels in the gap region. Phases containing more than 6% tungsten are semiconducting over the measurement range of 298–1.5 K. These strong effects are similar to what was observed in $K_{0.3}Mo_{1-x}W_xO_3$[26] and indicate that W substitution in the Mo polyhedra interferes with overlap of Mo t_{2g}4d and oxygen π2p orbitals, which determine the band structure.

The effect of alkali metal ion substitution on the electronic properties of $Li_{0.9}Mo_6O_{17}$ was studied in $(Li_{1-x}K_x)_{0.9}Mo_6O_{17}$ and $(Li_{1-x}Na_x)_{0.9}Mo_6O_{17}$ phases.[36,116,123] Substantial Na and K content merely broadens the metal-to-metal transition at 24 K and the superconducting state is still observed at ~2 K for $x \leq 0.4$ and $x \leq 0.48$, respectively (Figure 24). This is taken as strong evidence that the transition at 24 K is electron–phonon mediated and driven by a CDW (or SDW) instability primarily due to the anisotropic Fermi surface of the quasi-2D (or quasi-1D) Mo_6O_{17} lattice, rather than a localization due to disorder (Anderson type).

The only study of pressure effects on the electronic properties of the purple bronzes was carried out on $K_{0.9}Mo_6O_{17}$.[130] These data indicated that the room temperature resistivity decreased under pressure, which may be consistent with a semimetallic behavior; the pressure increases the overlap of the highest occupied bands and therefore the carrier concentration. The temperature of the onset of the CDW appears to be decreased by low applied pressure ($P \sim 0.50$ GPa), similar to what has been found in layered dichalcogenides[131] and where it has been attributed to the distortion of the Fermi surface under pressure. The nesting of the Fermi surface, responsible for the CDW would be reduced by the pressure and therefore the onset temperature decreased. At low temperature, the increase of the resistivity under pressure (Figure 25) suggests a semiconducting-type behavior which may indicate a weak localization of carriers due to pressure-induced defects. This is similar to the low-tem-

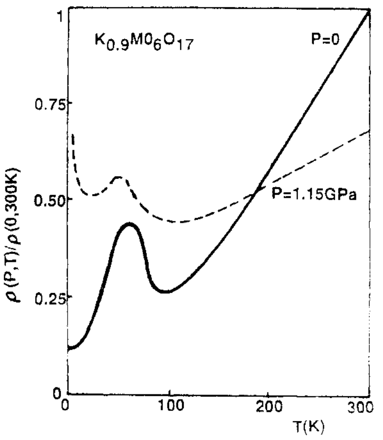

Figure 25. Resistivity vs temperature at zero pressure and at 1.15 GPa for $K_{0.9}Mo_6O_{17}$. The resistivity is measured in the plane perpendicular to the *c* axis (after ref 130).

perature properties of the Fe-doped $K_{0.9}Mo_6O_{17}$ under zero pressure[130] and also to that of $Na_{0.9}Mo_6O_{17}$ where impurities and defects may be responsible for the increase in ρ and χ seen at low temperature, due to weak Anderson localization.

The electronic properties of potassium molybdenum purple bronze, $K_{0.9}Mo_6O_{17}$, were recently examined by a tight-binding calculation on a single Mo_6O_7 layer.[132] The calculations show the presence of three partially filled d-block bands, which are essentially derived from the t_{2g} orbitals of the MoO_6 octahedra (Mo(2) of Figure 10 with oxidation state 5.1) belonging to the innermost two sublayers of Mo_6O_{17}. Figure 26a shows the bottom portion of the d-block bands of the real Mo_6O_{17} layer.[58] The Fermi surfaces (Figure 26b–d) of the three partially filled bands show that $K_{0.9}Mo_6O_{17}$ is a 2D metal, its CDW at 120 K results from the nesting of one of the three Fermi surfaces (Figure 26d), and the remaining two provide electron and hole carriers below 120 K. The band calculations are also valid for $Na_{0.9}Mo_6O_{17}$ and $TlMo_6O_{17}$, which are isostructural with $K_{0.9}Mo_6O_{17}$.

Preliminary results of a similar tight-binding calculation on $Li_{0.9}Mo_6O_{17}$ indicate that this material is a quasi-1D metal, because two partially filled d-block bands originate primarily from the –Mo(1)–O–Mo(4)–O– double chains extending along the *b* axis.[132] The two partially filled bands are dispersive along the chain direction (primarily along the *b* axis). Each of these two bands provides a 1D Fermi surface nested by a vector $q \simeq (0, 0.45b^*, 0)$. Therefore, the band calculations suggest that $Li_{0.9}Mo_6O_{17}$ is susceptible to either a CDW or SDW formation associated with the nesting vector.[132] According to Fröhlich, sliding CDW can lead to superconductivity.[75] In general, Fröhlich superconductivity is not observed because of CDW pinning, which gives rise to nonlinear conductivity. If a CDW is responsible for the resistivity upturn at ~24 K, the absence of nonlinear conductivity in $Li_{0.9}Mo_6O_{17}$ implies that CDW pinning might not occur in this compound. It is possible that superconductivity at 1.9 K is the consequence of Fröhlich mechanism rather than the normal BCS mechanism. However, observation of both the resistivity upturn att ~24 K and superconductivity at ~2 K in $(Li_{1-x}Na_x)_{0.9}Mo_6O_{17}$ ($x \leq 0.48$) and $(Li_{1-x}K_x)_{0.9}Mo_6O_{17}$ ($x \leq 0.40$), despite random potentials expected due to the presence of mixed alkali metal ions, is inconsistent with the formation of a sliding CDW at ~24 K. The absence of anomaly in the magnetic susceptibility of $Li_{0.9}Mo_6O_{17}$ down to 4.2 K, however, is consistent with a SDW instability being responsible for the resistivity upturn at ~24 K.[132]

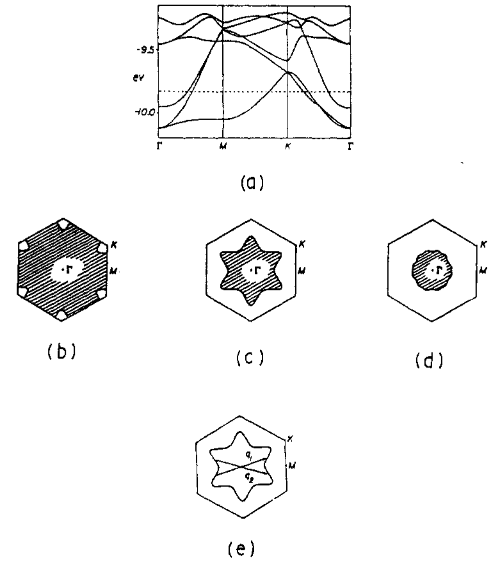

Figure 26. (a) Bottom portion of the d-block bands of the real Mo_6O_{17} layer of $K_{0.9}Mo_6O_{17}$. (b–d) Fermi surfaces for the first, second, and third d-block bands (from the bottom) of the Mo_6O_{17} layer. (e) Two pairs of nested pieces of the Fermi surface associated with the second d-block band of Mo_6O_{17} layer. (a–e after ref 58.)

We have looked for nonlinearity of the *I–V* characteristics in all of the purple bronzes, but detected only linear behavior. These materials are very conducting below the transition temperature and the maximum threshol voltages that can be achieved are small (<100 mV/cm).

VI. The Red Bronzes ($A_{0.33}MoO_3$)

Wold et al. reported on the preparation of the first red molybdenum bronze, $K_{0.33}MoO_3$, by fused-salt electrolysis.[14] They found $K_{0.33}MoO_3$ to be semiconducting with a positive temperature dependence and a room temperature resistivity of $\sim 10^4$ Ω cm. Later, Bouchard et al. confirmed these results and showed that the susceptibility was nearly temperature independent and positive.[15] They attributed this behavior to spin pairing of the d electrons or the formation of Mo^{4+} ions (d^2) with low-spin configuration ($S = 0$). Stephenson and Wadsley determined the crystal stucture and showed that the monoclinic structure (space group $C2/m$) is built of infinite sheets of corner/edge-sharing distorted MoO_6 octahedra which are joined together by the K^+ ions which are in an irregular eightfold coordination.[133] The structure is very similar to that of the blue bronze except that in the red bronze the unit of structure is six edge-shared octahedra which then corner share along *b* and the [102] direction to form the infinite layers (Figure 27). If all the potassium sites are occupied, $K_{0.33}MoO_3 = K_2Mo_6O_{18}$, and hence two electrons per Mo_6O_{18} cluster. Dickens and Neild[53] measured the electronic spectra and showed the donor levels to be at least 0.75 eV below the bottom of the conduction band (Figure 1). They also measured the ESR spectra and found a well-resolved signal at $g \sim 1.96$, which they attributed to Mo^{5+} centers. ESR studies by Bang and Sperlich[134] indicated two types of resonances, one of

TABLE 4. Unit Cell Parameters of $A_{0.33}MoO_3$ Phases

	$Li_{0.33}MoO_3$[a]	$K_{0.33}MoO_3$[b]	$Tl_{0.33}MoO_3$[c]	$Rb_{0.33}MoO_3$[d]	$Cs_{0.33}MoO_3$[e]
color	blue	red	red	red	red
unit cell	triclinic	monoclinic	monoclinic	monoclinic	monoclinic
space group	$P\bar{1}$	$C2/m$	$C2/m$	$C2/m$	$C2/m$
a, Å	13.079 (2)	14.278 (8)	14.537 (1) (14.541 (3))	14.809 (8)	15.862 (2)
b, Å	15.453 (2)	7.723 (5)	7.7230 (5) (7.780 (2))	7.726 (5)	7.728 (2)
c, Å	7.476 (1)	6.387 (4)	6.4096 (4) (6.414 (2))	6.410 (4)	6.4080 (7)
α, deg	96.97 (2)				
β, deg	106.56 (2)	92.34	93.096 (5) (93.09 (2))	93.8 (5)	94.37 (1)
γ, deg	103.368 (9)				

[a] Reference 138. [b] Reference 63. [c] Reference 34; values in parentheses reported by ref 114. [d] Reference 31. [e] Reference 141.

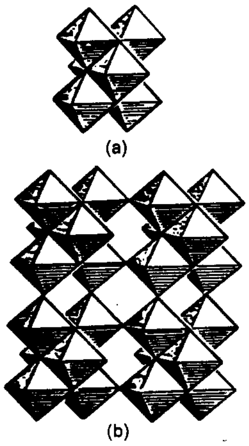

Figure 27. Idealized structure of $K_{0.33}MoO_3$ (after ref 134).

which was assigned to unpaired d electrons delocalized over six MoO_6 octahedra (i.e., in one cluster) while the other was assigned to pairs of exchanged coupled d electrons.[135]

More recently, Travaglini et al.[136] measured the optical reflectivity of $K_{0.33}MoO_3$ single crystals in the infrared and visible range in the temperature range 4–300 K using polarized light. These data indicated that this compound is a 0.5-eV energy gap semiconductor with very strong anisotropy in the infrared and visible range. These investigators derived a microscopic model to explain the metal–semiconductor "transition" between the blue bronze and the red bronze in terms of a formal Mott transition.[137] This is attributed to the substantial elongation of Mo–O bond distances along the b axis in $K_{0.33}MoO_3$ compared to those in $K_{0.3}MoO_3$ such that the dt_{2g}–$p\pi$, Mo–O–Mo overlap is less than necessary for delocalization. It would be interesting to see the effect of pressure along the b axis on the electrical properties.

Reau et al. reported on the red bronze $Rb_{0.33}MoO_3$, which, based on its unit cell parameters, appears to be isostructural with the K analogue.[31] In another communication these authors reported on a blue-violet monoclinic phase, Li_xMoO_3 ($0.31 \leq x \leq 0.39$), which they prepared by a solid-state reaction. Later, single crystals of a blue-violet bronze, $Li_{0.33}MoO_3$, prepared by electrolysis were shown to be the same phase as the one reported by Reau et al. and shown to be a semiconducting with a room temperature resistivity of 10^5 Ω cm.[20] More recently, large single crystals of $Li_{0.33}MoO_3$ have been prepared by the gradient flux technique.[32] An X-ray crystal structure determination by Tsai et al.[138] showed that this bronze is triclinic, not monoclinic as previously reported. The structure is completely different from that of the K and Rb red bronzes, forming a 3D network of corner- and edge-sharing distorted MoO_6 and LiO_6 octahedra. The location of lithium atoms at completely occupied octahedral sites establishes the stoichiometric composition $Li_{0.33}MoO_3 = LiMo_3O_9$. Along the c direction MoO_6 octahedra are connected by corner sharing to form infinite chains and the Mo–O–Mo bond distances are regular within the critical distance[138] for good dt_{2g}–$p\pi$ overlap. Furthermore, bond length–bond strength type calculations[139] show the unpaired 4d electrons on molybdenums in this chain. Although the electrical conductivity is highest along this direction, the behavior is semiconducting.[37]

The structure of the thallium analogue of $A_{0.33}MoO_3$ red bronzes was determined recently.[140] $Tl_{0.33}MoO_3$ is isostructural with the K and Rb phases; it is a p-type semiconductor and ρ at room temperature is $\sim 10^5$ Ω cm as in the other red bronzes.[34,140] Unit cell parameters of the known $A_{0.33}MoO_3$ phases are listed in Table 4. As in the blue bronzes, a, c, and β increase fairly regularly with increasing size of the A^+ cation in the isostructural monoclinic phases (K, Tl, Rb, Cs) while b remains remarkably constant but significantly larger than b in $K_{0.3}MoO_3$ (Table 1). The c dimension in $Li_{0.33}MoO_3$, corresponding to the direction of chains of corner-sharing MoO_6 octahedra in this bronze, is surprisingly short, in fact shorter than b in the blue bronzes. However, metallic behavior is not observed along this direction, probably because of band filling.

Reid and Watts prepared monoclinic copper-colored Cs_xMoO_3 bronzes by fused-salt electrolysis.[19] The X-ray crystal structure of this phase, corresponding to a $Cs_{0.25}MoO_3$ composition, was shown to be similar to but not identical with that of $K_{0.33}MoO_3$ by Mumm and Watts.[18] Strobel and Greenblatt prepared a red bronze, $Cs_{0.33}MoO_3$, also by fused-salt electrolysis and showed it to be semiconducting with $\rho \sim 10^5$ Ω cm at room temperature;[20] when this bronze was ground into a powder, it turned blue and the powder pattern could not be indexed with the cell parameters reported for a red Cs bronze by Mumme and Watts.[18] More recently, $Cs_{0.33}MoO_3$ red bronze crystals were grown by the gradient flux technique by Ramanujachary et al.[33] An X-ray structure analysis showed that this phase is isostructural with $K_{0.33}MoO_3$;[141] moreover, the X-ray powder pattern of the polycrystalline blue phase which results upon grinding of the red bronze crystals could be indexed with the lattice parameters determined by

TABLE 5. Crystallographic Data for Cs_xMoO_3 Bronzes

compd	color	a, Å	b, Å	c, Å	β, deg	space group	ref
$Cs_{0.33}MoO_3$	red	15.862 (2)	7.728 (2)	6.4080 (7)	94.37 (1)	*C*2/*m*	141
$Cs_{0.25}MoO_3$	copper	6.425 (5)	7.543 (5)	8.169 (5)	96.50 (5)	$P2_1$ or $P2_1/m$	18
$Cs_{0.25}MoO_3$[a]	blue	19.063 (5)	5.5827 (23)	12.1147 (23)	118.94 (2)	*C*2/*m*	143

[a] Formula may be represented as $CsMo_{4-x}O_{12}$ ($x \simeq 0.13$).

TABLE 6. Unit Cell Dimensions of H_xMoO_3 Bronze Phases

compd	color	a, Å	b, Å	c, Å	β, deg	space group	ref
$H_{0.34}MoO_3$	blue	3.896	14.07	3.736	90.0	*Cmcm*	48
$H_{0.93}MoO_3$	blue	14.53	3.796	3.864	93.74	monoclinic	48
$H_{1.68}MoO_3$	red	13.97	3.770	4.055	93.97	monoclinic	48
$H_{2.0}MoO_3$	green	13.55	3.897	4.053	94.63	monoclinic	48
MoO_3[a]		3.962	13.86	3.697	90.0		42

[a] *a*,*b*,*c* orthorhombic → *b*,*a*,*c* monoclinic.

this structural investigation.

Differential scanning calorimeter (DSC) measurements at high pressure indicate a phase transition at 553 °C and 100-psi pressure; T_c decreases with increasing pressure.[142] The pressure variation of resistivity at room temperature, with the pressure applied perpendicular to the platelet direction of a single crystal of $Cs_{0.33}MoO_3$, indicates a phase transition at about the pressure expected from the DSC results. The resistivity of $Cs_{0.33}MoO_3$ decreases by several orders of magnitude with increasing pressure.[142] Measurements of ρ vs P at various temperatures are in progress.[142]

A blue $Cs_{0.19}MoO_3$ semiconducting phase appears to be yet another structurally different Cs–Mo–O phase.[23] A redetermination of the composition by elemental analysis as well as a structural determination by X-ray diffraction indicates that the actual stoichiometry is $Cs_{0.25}MoO_3$.[143] This phase is monoclinic with a unit cell that bears no obvious relationship to the unit cells of other alkali metal molybdenum bronzes (Table 4). The structural determination confirmed that $Cs_{0.25}MoO_3$ has a completely different structure than the $A_{0.3}MoO_3$ blue bronzes.[143] The anomalies in the susceptibility and the resistivity vs temperature suggest that this material undergoes a phase transition near 200 K. The susceptibility anomaly is similar in shape and even the temperature at which it occurs to the anomaly observed in the $A_{0.3}MoO_3$ blue bronzes.[23] However, the resistivity of $Cs_{0.25}MoO_3$ is semiconducting above as well as below the anomaly. Consequently, if the sample is single phase, this transition cannot be due to a CDW. Unit cell parameters of the different semiconducting Cs–Mo–O phases are summarized in Table 5. The question of whether or not there are two structurally different red Cs–Mo–O bronze phases remains unresolved.

VII. Hydrogen Molybdenum Bronzes

MoO_3 has a unique layer structure in which infinite chains of corner-sharing MoO_6 octahedra are fused together by edge sharing to form corrugated layers;[144] the layers are stacked parallel to one another and are held together by van der Waals forces (Figure 28). The Mo–O distances along the O(2)–Mo–O(2′) corner-sharing direction of the MoO_6 octahedra are distorted to form alternate long, 2.25-Å bonds and short, 1.73-Å bonds. At ambient temperature chemical reduction using metal/H^+ couples (e.g., Zn/HCl)[41] or electrochemical reduction in aqueous acidic media[45] (MoO_3 + $xH^+ + xe^- \rightarrow H_xMoO_3$) leads to the formation of hydrogen molybdenum bronzes, H_xMoO_3 with $0 < x \leq 2$.

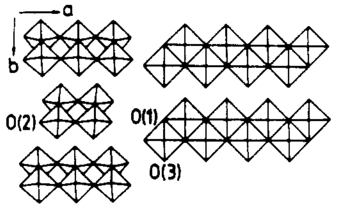

Figure 28. Schematic diagram of the structure of MoO_3 (after ref 51).

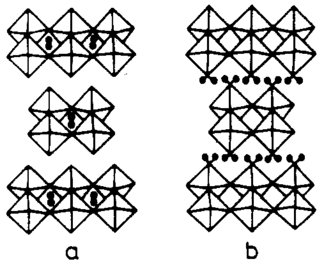

Figure 29. Schematic structures of (a) $H_{0.36}MoO_3$ and (b) $H_{1.68}MoO_3$ (after ref 51).

The existence of a series of hydrogen molybdenum bronzes H_xMoO_3 was first reported by Glemser et al.[41] A more complete investigation by Birtill and Dickens[47] indicated the presence of four distinct phases in H_xMoO_3 for $0 < x \leq 2$. Ranges of homogeneity exist for three of these phases with the following approximate limits: blue, orthorhombic, $0.23 < x < 0.4$; blue, monoclinic, $0.85 < x < 1.04$; red, monoclinic, $1.55 < x < 1.72$. The green, monoclinic fourth phase with $x = 2.0$ appears to have fixed composition. Unit cell parameters of typical compositions of these phases along with that of MoO_3 are given in Table 6. Comparison of their lattice parameters with those of MoO_3 indicates that hydrogen is inserted into the MoO_3 matrix with minimal structural rearrangement.

A powder neutron diffraction study of $D_{0.36}MoO_3$ has shown that the deuterium atoms are attached to the bridging oxygen atoms O(2) as O–D groups (Figure 29a).[48] In $H_{0.36}MoO_3$ the distortion involving the bridging oxygens is removed, and two symmetrical Mo–O(2) bonds, each 1.96 Å long, are formed. The presence of OH groups is also supported by the inelastic neutron scattering spectra of $H_{0.34}MoO_3$, where an absorption at 1267 cm^{-1} may be assigned to an Mo–O–H bend.[48] For the monoclinic phases $H_{0.93}MoO_3$, $H_{1.68}$-

MoO_3, and $H_{2.0}MoO_3$, inelastic neutron scattering studies show only peaks associated with OH_2 groups as evidenced by a strong peak at 1620 cm^{-1}.[48] Moreover, a powder neutron diffraction study of $D_{1.68}MoO_3$ revealed that the deuterium atoms are attached to the terminal oxygen atoms, O(3) in MoO_3, as OD_2 groups (Figure 29b).[51] The Mo–O(3) bond is substantially longer (2.18 Å) in the $D_{1.68}MoO_3$ compound than in MoO_3 (1.68 Å), indicating reduction of π bonding in the Mo–O(3) bond due to formation of O(3)–D_2 bonds. The arrangements of the hydrogen atoms in $H_{0.36}MoO_3$ and $H_{1.68}MoO_3$ shown in Figure 29 are also consistent with the second-moment values obtained from NMR measurements.[145]

The H_xMoO_3 phases are deeply colored, mixed ionic/electronic conductors. They exhibit metallic properties with weak, temperature-independent paramagnetism and no ESR signal down to 4.2 K.[146,147] These results suggest that the electronic structure of H_xMoO_3 phases is similar to that of other metallic molybdenum bronzes discussed above, with partially occupied metal dt_{2g}–oxygen $2p\pi$ bands.

Proton mobilty in H_xMoO_3 has been studied by NMR techniques.[45,145,148] Only $H_{1.7}MoO_3$ shows substantial proton mobility with $D(298\ K) = 10^{-8}\ cm^2\ s^{-1}$.[145,148] Diffusion of protons between layers (Figure 29b) probably takes place via a Grotthus type mechanism.[51]

The properties of H_xMoO_3 bronzes have led to their investigation for possible applications as gas sensors,[149] electrochromic materials,[150] hydrogen storage materials,[151] and hydrogenation catalysts.[152]

VIII. Molybdenum Oxides: η-Mo_4O_{11}, γ-Mo_4O_{11}, and Mo_nO_{3n-1} Magnelí Phases

A. Introduction

Although these are binary molybdenum compounds, they exhibit bronze-like structural and physical properties. The Mo_4O_{11} phases are very similar to the purple bronzes both in their structural and in their physical properties.[27] However, in contrast to the purple bronzes, these compounds undergo a CDW transition to an incommensurate state. Mo_8O_{23} is a member of the Mo_nO_{3n-1} homologous series of oxides and the first example of this class of materials to show quasi-low-dimensional transport behavior.[153] Higher members of this series, Mo_9O_{26} and $(Mo_{0.88}W_{0.12})_{10}O_{29}$, also indicate a CDW-driven phase transition.[154]

B. Structure

Mo_4O_{11} forms in a high-temperature orthorhombic γ phase and low-temperature monoclinic η phase; the transition temperature $\gamma \rightarrow \eta$ is ~610 °C.[155] Refinements of the crystal structures have been performed for both types by Kihlborg[114] and a rerefinement of the γ-Mo_4O_{11} has been reported recently by Ghedira et al.[156] In both the γ and η structures, there are four independent Mo sites: Mo(1) occupies the tetrahedral site while Mo(2), Mo(3), and Mo(4) are located in octahedral positions. The MoO_6 octahedra corner share to form infinite three-octahedra-thick slabs which are connected by MoO_4 tetrahedra. The cation charges are 5.99, 5.85, 5.40, and 5.02 for Mo(1), Mo(2), Mo(3), and Mo(4), respectively; thus the 4d electrons are located in slabs, which are parallel to the (*bc*) plane, the plane of high conductivity. The structure is very similar to that of the $A_{0.9}Mo_6O_{17}$ system (Figure 10), except that the alkali metals are absent and the tetrahedral planes are connected to form a three-dimensional network structure of Mo polyhedra. The *a* axis of Mo_4O_{11} corresponds to the *c* axis of the purple bronzes. In η-Mo_4O_{11} two consecutive slabs are identical, while in γ-Mo_4O_{11} they are mirror images of one another as shown in Figure 30.

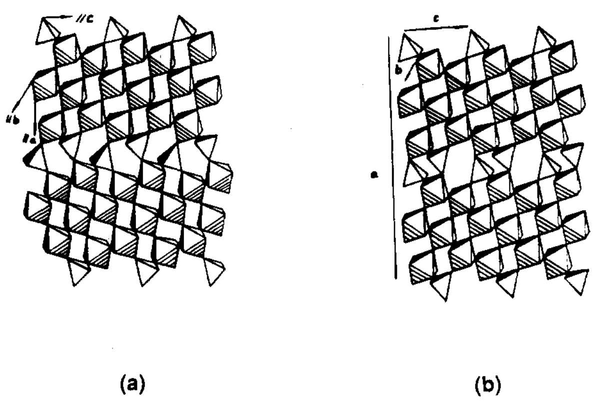
(a) (b)

Figure 30. Idealized structures of (a) η-Mo_4O_{11} and (b) γ-Mo_4O_{11}, showing MoO_6 octahedral slabs and MoO_4 tetrahedral planes (after ref 27).

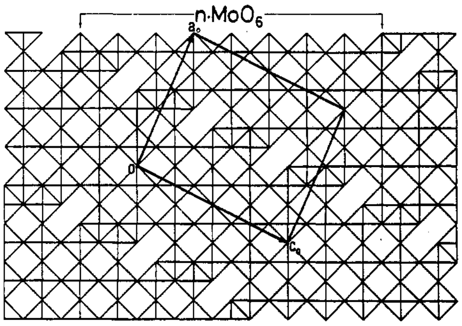

Figure 31. Schematic structure of Mo_nO_{3n-1} (here $n = 9$) projected along the [010] direction (after ref 155e).

The structure of Mo_8O_{23} was determined by Magneli long ago[157] and refined by others.[114] The structure of Mo_nO_{3n-1} phases in general can be described as built up of corner-sharing MoO_6 octahedra forming blocks of ReO_3 type which extend infinitely through the crystal in two dimensions and have a finite characteristic width of *n* octahedra in the third direction; the blocks are mutually joined by octahedra sharing edges as shown in Figure 31.[155e]

Recently, the structural properties of Mo_8O_{23} have been determined by single-crystal X-ray diffraction at 360 and 100 K, respectively.[154d] Mo_8O_{23} has an incommensurate structure at room temperature, and an incommensurate–commensurate phase transition takes place at about 285 K. The structure of the normal phase at 370 K is essentially the same as that presented by Magneli for room temperature. The structure of the commensurate phase at 100 K can be described mainly by the inhomogeneous rotations of MoO_6 octahedra.

More recently, detailed single-crystal X-ray structural studies were carried out for Mo_9O_{26} and $(Mo_{0.88}W_{0.12})_{10}O_{29}$, respectively.[155e] A structural phase transition is observed at 500 K for Mo_9O_{26} and at 612 K for the $(Mo_{0.88}W_{0.12})_{10}O_{29}$ phase. Superlattice peaks observed at room temperature at (0.5, 0.5, 0.0) for Mo_9O_{26}

TABLE 7. Unit Cell Dimensions of Mo_4O_{11} and Mo_nO_{3n-1} (n = 8–10)

compd	crystal system	a, Å	b, Å	c, Å	β, deg	space group	ref
γ-Mo_4O_{11}	orthorhombic	24.487 (1)	5.457 (1)	6.752 (1)		$Pn2_1a$	156
η-Mo_4O_{11}	monoclinic	24.54	5.439	6.701	94.28	$P2_1/a$	114b
Mo_8O_{23}	monoclinic	13.4	4.04	16.8	106.1	$P2/c$	157
Mo_9O_{26}	monoclinic	29.194 (3)	8.083 (1)	16.816 (3)	95.47 (1)	$C2/c$	155e
$(Mo_{0.88}W_{0.12})_{10}O_{29}$		17.437 (3)	8.029 (1)	16.787 (3)	111.70 (1)	$P2/c$	155e

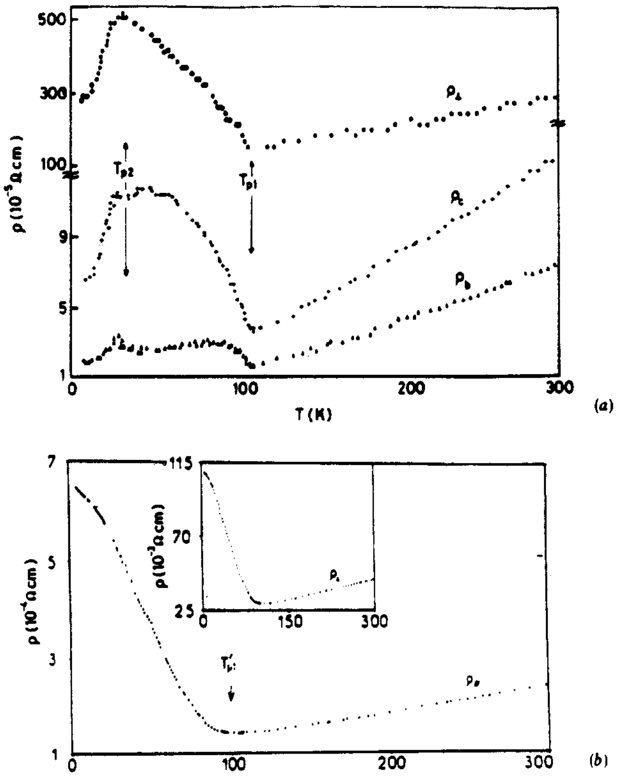

Figure 32. Temperature variation of the resistivity of (a) η-Mo_4O_{11} along the a, b, and c axes (after ref 160) and (b) γ-Mo_4O_{11} in a direction parallel and perpendicular to the slabs (after ref 159b).

and at (0.0, 0.5, 0.0) for $(Mo_{0.88}W_{0.12})_{10}O_{29}$ are not detected above the transition temperatures in either phase. This suggests that the transitions take place from the high-temperature phase (T > 500 and 612 K, respectively) to the commensurate phases directly. Room temperature unit cell dimensions and space group information of the Mo_4O_{11} and Mo_nO_{3n-1} phases discussed here are given in Table 7.

C. Charge Density Wave Instabilities

The transport properties and magnetic susceptibility of both γ- and η-Mo_4O_{11} have been measured on powder samples by Gruber et al.[158] Single-crystal studies of the anisotropy of the electrical resistivity, thermopower, magnetic susceptibility, and specific heat measurement of both compounds show evidence of CDW instabilities. The temperature dependence of the resistivity (Figure 32) and of the magnetic susceptibility (Figure 33) is highly anisotropic and shows metallic behavior below the transition for both phases. However, the resistivity of γ-Mo_4O_{11} increases below the onset of CDW at T_c = 100 K.[23,153a,159] to the lowest temperatures while in η-Mo_4O_{11}, ρ shows a maximum at T_{c1} = 109 K and a second transition at T_{c2} = 30 K, particularly evident as a small peak in the resistivity along b (Figure 32).[160]

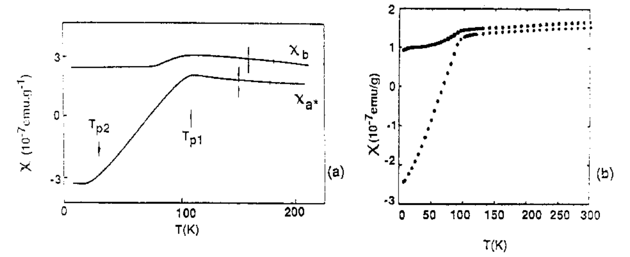

Figure 33. (a) Magnetic susceptibility of η-Mo_4O_{11} corrected for the Curie contribution as a function of temperature. The magnetic field is parallel to the b or a^* axis (after ref 27). (b) Magnetic susceptibility corrected for the Curie–Weiss contribution: bottom curve, parallel to the a axis; top curve, perpendicular to the a axis (after ref 159c).

As in the purple bronzes, the resistivity along the a axis ($\rho_\perp$) is 50–100 times greater than in the (bc) plane ($\rho_\parallel$), indicating quasi-2D metallic behavior. These properties are well accounted for by the crystal structure in which the 4d electrons are confined in the MoO_6 octahedral layers (as in the $A_{0.9}Mo_6O_{17}$ phases) well separated from each other by MoO_4 tetrahedra. This should result in an anisotropic and quasi-cylindrical Fermi surface with large areas parallel to a^*. The nesting therefore affects only small portions of the surface and induces only partial gaps at the transition. This increases the resistivity below T_c, but the compounds remain metallic, similar to the purple bronzes.

The main difference between the two compounds is the temperature dependence at the CDW gaps: in η-Mo_4O_{11} the opening of the gaps appears, to be complete near 50 K,[160] and the Fermi surface undergoes a second instability, corresponding to the second transition. In γ-Mo_4O_{11}, the gaps continue to open up down to 4.2 K.[159b] Despite the slight difference of structure, the conduction electron concentration, the Fermi surface, and the band structure are expected to be very similar in the two compounds; therefore the differences observed may be due to different electron–phonon coupling strengths. Analogous variations in the behavior of different $A_{0.9}Mo_6O_{17}$ compounds were also attributed to differences in electron–phonon coupling effects.[36]

In both compounds, the magnetic susceptibility shows a strong anisotropy below the onset of CDW (Figure 33).[159–161] The susceptibility is attributed to Pauli and Van Vleck paramagnetism and to core and the free-electron Landau diamagnetism; the small values of χ are due to a partial compensation between these contributions. The large anisotropy below T_c is probably due to a large anisotropy of the Landau diamagnetism associated with closed orbits in the (bc) plane.[160–161]

The thermopower S in both compounds is negative and linear with temperature from 300 K to T_c. The temperature variation of S of η-Mo_4O_{11} is shown in Figure 34. Below T_c, $|S(T)|$ shows a large increase and a maximum which may indicate the contribution of charge carriers of both signs. Although the dominant

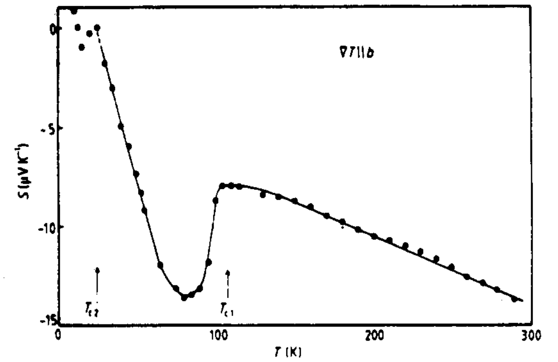

Figure 34. Thermopower of η-Mo_4O_{11} as a function of temperature (after ref 160).

carriers are always electrons, the contribution of holes becomes more important at lower temperatures ($T <$ 50 K). This is consistent with the presence of electron and hole pockets left by the opening of CDW gaps. A second transition (T_{c2}) seen in the resistivity and susceptibility of η-Mo_4O_{11} also shows an anomaly in $S(T)$ below T_{c2}.[160]

The CDW transitions have also been studied by specific heat measurements.[159b,160] In γ-Mo_4O_{11} the CDW transition at ~100 K could not be detected.[159b] However, both transitions were observed in the C_p vs T data of η-Mo_4O_{11}.[160] The thermal data obtained from these measurements are summarized in Table 3. The Debye temperature θ_D of 330 K found for η-Mo_4O_{11} is significantly lower than $\theta_D = 418$ K of γ-Mo_4O_{11}, which shows that the lattice rigidity is stronger in the latter; this corroborates the presence of larger electron–phonon interactions in γ-Mo_4O_{11} and the opening of gaps down to 4.2 K. This is also consistent with the fact that the γ phase is the stable phase at high temperature.[155] The nonzero value of γ coefficient for both compounds clearly establishes that the low-temperature phases are metallic and therefore the negative temperature coefficient of the resistivity below T_c is due to a partial opening of gaps at the Fermi surface. Furthermore, from the γ values, rough estimates of the density of states, $g(E_F)$ at the Fermi level in the low-temperature phase compared to $g(E_F)$ calculated from the temperature dependence of the thermopower above T_c indicate that the opening of CDW gaps lead to significant decrease of the density of states at the Fermi level.[159b,160] X-ray diffuse scattering and electron diffraction studies show the presence of weak incommensurate superlattice spots below T_c[161] in contrast to the purple bronzes which are characterized by a commensurate CDW.

The wave vector component along b^* is $q_b = 0.23 \pm 0.015$ in both Mo_4O_{11} compounds, which supports the previous contention that the Fermi surfaces of both compounds are similar. However, nonlinear transport due to the sliding of incommensurate CDW have not been observed in these oxides so far.

The magnetotransport properties of η-Mo_4O_{11} also corroborate the anisotropic 2D properties of the Fermi surface and show that the gap openings at the transition leave very small electron and hole pockets.[159a,161]

Sato et al.[153] studied the temperature dependence of electrial resistivity in Mo_8O_{23} (Figure 35). The resistivity is highly anisotropic indicative of possible quasi-1D behavior. The high-temperature behavior appears to be metallic, and a CDW-like transition occurs in the vicinity of 200 K. The resistivity peaks near 150 K along all three crystallographic directions. The increase in the resistivity at low temperatures is attributed to localization effects. The magnetic susceptibility of a polycrystalline sample (Figure 36) shows a sharp decrease in the susceptibility corresponding to the transition in the resistivity. Similar anisotropies and anomalies can be seen in the temperature dependence of resistivity (Figure 35) and susceptibility of Mo_9O_{26}. $(Mo_{0.88}W_{0.12})_{10}O_{29}$ appears to be semiconducting (Figure 35).[154e]

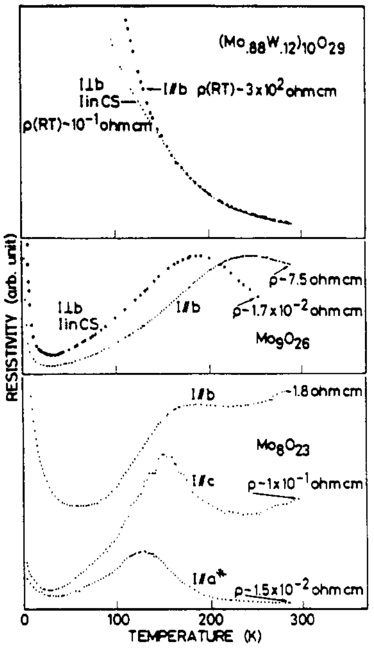

Figure 35. Temperature variation of the resistivity of Mo_nO_{3n-1} along the principal directions. Rough values of the specific resistivities are indicated at the corresponding temperatures. Here the x axis is defined in the crystallographic shear plane (after ref 154b).

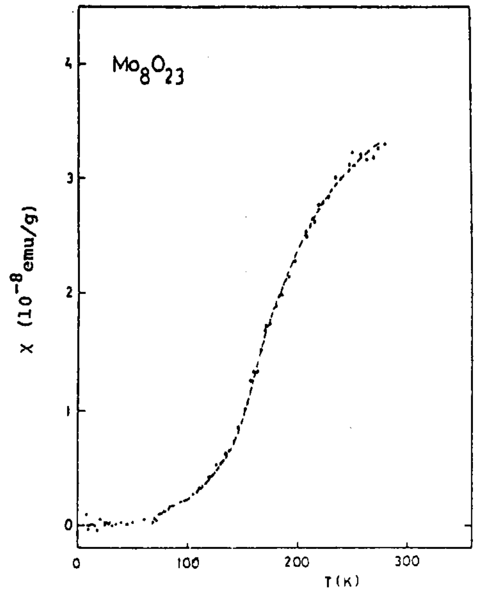

Figure 36. Temperature dependence of the magnetic susceptibility of Mo_8O_{23}. The T-independent diamagnetic part and the Curie paramagnetic part due to lattice imperfections have been subtracted (after ref 153a).

The anomalous temperature dependence of resistivity in Mo_8O_{23} and Mo_9O_{25}, the observation of superlattice

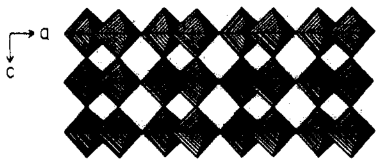

Figure 37. A section of the $La_2Mo_2O_7$ structure showing corner sharing of Mo_2O_{10} in the crystallographic *ac* plane (after ref 163).

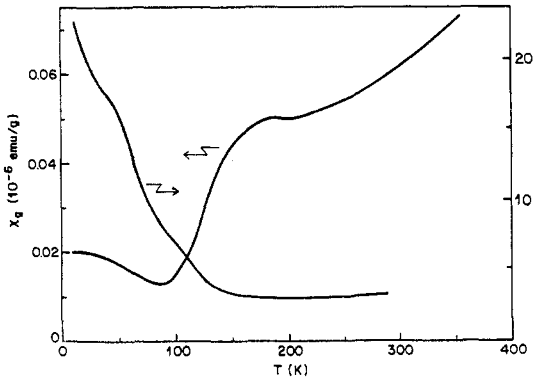

Figure 38. Temperature variation of the resistivity and magnetic susceptibility of $La_2Mo_2O_7$ (corrected for paramagnetic impurities) (after ref 163).

reflections below the critical temperature in all three Mo_nO_{3n-1} (n = 8, 9, 10) compounds support formation of CDW in all these phases.

IX. $La_2Mo_2O_7$: A Rare-Earth Molybdenum Bronze

Recently, single crystals of the purple, bronze-like $La_2Mo_2O_7$ were grown by fused-salt electrolysis.[162] A single-crystal structure determination showed that the basic building blocks of the structure are two MoO_6 octahedral which share a common edge to form a fused Mo_2O_{10} unit. These units then share corners to form Mo–O layers as shown in Figure 37.[163] The layers are held together by the lanthanum ions. Although the structure is 3D overall, it can be considered as 2D with respect to the Mo–O network. The Mo–Mo distance in the Mo_2O_{10} groups is 2.478 Å, one of the shortest Mo–Mo distances thus far reported in molybdenum oxide systems (the reported Mo–Mo distance in $LiMoO_2$ is 2.46 Å, the only shorter reported Mo–Mo bond[164]).

$La_2Mo_2O_7$ has a room temperature resistivity of about 10^{-3} Ω cm.[165] The positive coefficient of the temperature dependence of the resistivity above 200 K indicates metallic behavior. A large increase in the resistivity (Figure 38) at 125 K is probably associated with a phase transition. This anomaly shows up in the magnetic susceptibility, which indicates weakly temperature dependent Pauli paramagnetic behavior above the transition temperautre (Figure 38).[163] Recent measurements of the electrical resistivity along the three unit cell directions showed that $\rho_a \simeq 6.4 \times 10^{-2}$ Ω cm, $\rho_b \simeq 5.2 \times 10^{-2}$ Ω cm, and $\rho_c \simeq 4 \times 10^{-3}$ Ω.[165] The high conductivity along the *c* axis is expected by the structural properties. The lowest conductivity direction, along *b*, is also predicted by the structure due to the absence of Mo–O–Mo interactions between planes of MoO_6 octahedra.

The band structure of $La_2Mo_2O_7$ recently determined by Whangbo and Canadell[166] by tight-binding calculations (Figure 39) reveals two partially filled d-block bands. The Fermi surfaces of these bands lead to nesting. The charge-density wave associated with these nesting vectors is likely to be responsible for the phase transition in $La_2Mo_2O_7$, which occurs around 125 K.

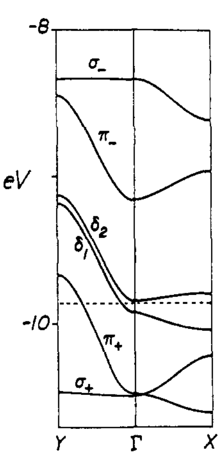

Figure 39. Six low-lying d-block bands for a 2D $Mo_2O_7^{6-}$ slab, where Γ, X, and Y are the wave vector points (0, 0), ($a^*/2$, 0), and 0, $c^*/2$), respectively, in the first Brillouin zone of the reciprocal space (i.e., Γ → X corresponds to the direction along *a*, and Γ → Y to that along c). The dashed line refers to the Fermi level (after ref 166).

Acknowledgments. The studies performed at Rutgers on the molybdenum bronzes would not have been possible without the many contributions of collaborators. W. H. McCarroll, while here on a sabbatical from Rider College, worked out the gradient flux technique for the crystal growth of the lithium bronzes and continued to guide and contribute to all aspects of the work here. Mark Croft and Rick Neifeld of the physics department helped us start the low-temperature resistivity measurements and were helpful in explaining the solid-state physics aspect of the problem. K. V. Ramanujachary, a postdoctoral fellow here for 3 years, grew some fine bronze crystals, built a computer-controlled state-of-the-art device for the measurement of the temperature variation of the resistivity and specific heat, and made important contributions in all areas of research, including the substitutional bronze studies. B. Collins, a Ph.D. candidate, worked out most aspects of Tl–Mo–O bronze results and contributed significantly to the substitutional studies. Many thanks to J. A. Potenza for his help in the single-crystal X-ray studies. F. J. DiSalvo was a constant source of help in interpreting the magnetic and electronic properties of the materials studied and a willing listener to test ideas on. We are grateful to J. V. Waszczak for measuring all the reported magnetic susceptibility data. The author would like to acknowledge P. G. Dickens, R. M. Fleming, C. Schlenker, L. F. Schneemeyer, and M.-H. Whangbo for their kind permission to reproduce some of their results. Finally, the support of the National Science Foundation Solid State Chemistry Grants DMR-81-15977, DMR-84-04003, and DMR-84-08266 and ONR support are gratefully acknowledged.

References

(1) (a) Wohler, F. *Ann. Chim. Phys.* **1825**, *29*, 43. (b) Wohler, F. *Philos. Mag.* **1825**, *66*, 263. (This is the English translation of (a).)
(2) Sienko, M. J. In *Non*-Stoichiometric *Compounds*; Gould, R. F., Ed.; Advances in Chemistry Series; American Chemical

Society: Washington, DC, 1963; p 224.
(3) Banks, E.; Wold, A. *Preparative Inorganic Reactions*; Jolly, W. L., Ed.; Interscience: New York, 1968; Vol. 4, p 237.
(4) Dickens, P. G.; Whittingham, M. S. *Q. Rev., Chem. Soc.* **1968**, *22*, 30.
(5) Hagenmuller, P. In *Progress in Solid State Chemistry*; Reiss, H., Ed.; Pergamon: New York, 1971; Vol. 5, p 71.
(6) Manthiram, A.; Gopalakrishnan, J. *Rev. Inorg. Chem.* **1984**, *6*, 1.
(7) Schlenker, C., Ed. *Low-Dimensional Properties of Molybdenum Bronzes* and *Oxidesf* Reidel: Dordrecht, to be published.
(8) Monceau, P.; Ong, N. P.; Portis, A. M.; Meerschaut, A.; Rouxel, J. *Phys. Rev. Lett.* **1976**, *37*, 602.
(9) For reviews, see: (a) Fleming, R. M. In *Physics in One Dimension*; Bernasconi, J., Schneider, T., Eds.; Springer Series in Solid State Sciences; Springer: Berlin, 1981; Vol. 23. (b) Ong, N. P. *Can. j. Phys.* **1982**, *60*, 757. (c) Monceau, P.; Richard, J.; Renard, M. *Phys. Rev. B: Condens. Matter* **1982**, *25*, 1931. (d) Richard, J.; Monceau, P.; Renard, M. *Phys. Rev. B: Condens. Matter* **1982**, *25*, 948. (e) Gruner, G. *Comments Solid State Phys.* **1983**, 10. (f) Gruner, G. *Physica D: (Amsterdam)* **1983**, *8D*, 1. (g) Monceau, P., Ed. *Electronic Properties of Inorganic Quasi-One-Dimensional Compounds*; In *Physics and Chemistry of Materials with Low-Dimensional Structures, Series B: Quasi-One-Dimensional Structures*, Reidel: Dordrecht, 1985. (h) Gruner, G.; Zettl, A. *Phys. Rev.* **1985**, *119*, 117.
(10) (a) Wang, Z. Z.; Saint-Lager, M. C.; Monceau, P.; Rendard, M.; Gressier, P.; Meerschaut, A.; Rouxel, J. *Solid State Commun.* **1983**, *46*, 325. (b) Meerschaut, A.; Rouxel, J. In *Crystal Chemistry and Properties of Materials with Quasi-One-Dimensional Structures*; Rouxel, J., Ed.; Reidel: Dordrecht, 1986; p 205. (c) Maki, M.; Kaiser, M.; Zettl, A.; Gruner, G. *Solid State Commun.* **1983**, *46*, 497.
(11) (a) Proceedings International Symposium on Non-Linear Transport and Related Phenomena in Inorganic Quasi-One-Dimensional Conductors, Hokkaido University, Sapporo, Japan, Oct 1983. (b) Proceedings International Conference on the Physics and Chemistry of Low Dimensional Synthetic Metals (ICSM 84), Abano Terme, Italy, June 1984 (*Mol. Cryst. Liq. Cryst.* **1985**, *121*. (c) Proceedings International Conference on Charge Density Waves in Solids, Budapest, Hungary, Sept 1984 (*Lect. Notes Phys.* **1985**, *217*). (d) Proceedings, Yamada Conference IX Physics and Chemistry of Quasi-One-Dimensional Conductors, Lake Kawaguchi, Japan, May 1986 (*Physica B+C: (Amsterdam)* **1986**, *143B+C*).
(12) (a) Schlenker, C.; Dumas, J. In *Crystal Chemistry and Properties of Materials with Quasi-One-Dimensional Structures*; Rouxel, J., Ed.; Reidel: Dordrecht, 1986; p 135. (b) Fleming, R. M. *Synth. Met.* **1986**, *13*, 241.
(13) Marcus, J.; Escribe-Filippini, C.; Chevalier, R.; Buder, R. *Solid State Commun.* **1987**, *62*, 221.
(14) Wold, A.; Kunnmann, W.; Arnott, R. J.; Ferretti, A. *Inorg. Chem.* **1964**, *3*, 545.
(15) Bouchard, G. H.; Perlstein, J.; Sienko, M. J. *Inorg. Chem.* **1967**, *6*, 1682.
(16) Perloff, D. S.; Vlasse, M.; Wold, A. *J. Phys. Chem. Solids, Suppl.* **1967**, *No. 1*, 361.
(17) Hagenmuller, P. *Preparative Methods in Solid State Chemistry*; Hagenmuller, P., Ed.; Academic: New York, 1972; p 279.
(18) Mumme, W. A.; Watts, J. A. *J. Solid State Chem.* **1970**, *2*, 16.
(19) Reid, A. F.; Watts, J. A. *J. Solid State Chem.* **1970**, *1*, 310.
(20) Strobel, P.; Greenblatt, M. *J. Solid State Chem.* **1981**, *36*, 331.
(21) Brusetti, R.; Chakraverty, B. K.; Devenyi, J.; Dumas, J.; Marcus, J.; Schlenker, C. In *Recent Developments in Condensed Matter Physics*; Devreese, J. T., Lemmens, L. F., Van Doren, V. E., Van Royen, J., Eds.; Plenum: New York, 1981; Vol. 2, p 181.
(22) Buder, R.; Devenyi, J.; Dumas, J.; Marcus, J.; Mercier, J.; Schlenker, C.; Vincent, H. *J. Phys. Lett.* **1982**, *43*, L59.
(23) Schneemeyer, L. F.; Spengler, S. E.; DiSalvo, F. J.; Waszczak, J. V.; Rice, C. E. *J. Solid State Chem.* **1984**, *55*, 158.
(24) Schneemeyer, L. F.; DiSalvo, F. J.; Fleming, R. M.; Waszczak, J. V. *J. Solid State Chem.* **1984**, *54*, 358.
(25) Pouget, J. P.; Kagoshima, S.; Schlenker, C.; Marcus, J. *J. Phys., Lett.* **1983**, *44*, L113.
(26) Schneemeyer, L. F.; DiSalvo, F. J.; Spengler, S. E.; Waszczak, J. V. *Phys. Rev. B: Condens. Matter* **1984**, *30*, 4297.
(27) Schlenker, C.; Dumas, J.; Escribe-Filippini, C.; Guyot, H.; Marcus, J.; Fourcaudot, J. *Philos. Mag. B*: **1985**, *52*, 643.
(28) Ganne, M.; Boumaza, A.; Dion, M.; Dumas, J. *Mater. Res. Bull.* **1985**, *20*, 1297.
(29) Reau, J.-M.; Fouassier, C.; Gleitzer, C.; Parmentier, M. *Bull. Soc. Chim. Fr.* **1970**, 479.
(30) Reau, J.-M.; Fouassier, C.; Hagenmuller, P. *J. Solid State Chem.* **1970**, *1*, 326.
(31) Reau, J.-M.; Fouassier, C.; Hagenmuller, P. *Bull. Soc. Chim. Fr.* **1971**, 2883.
(32) McCarroll, W. H.; Greenblatt, M. *J. Solid State Chem.* **1984**, *54*, 282.
(33) Ramanujachary, K. V.; Greenblatt, M.; McCarroll, W. H. *J. Cryst. Growth* **1984**, *70*, 476.
(34) Collins, B. T.; Ramanujachary, K. V.; Greenblatt, M.; Waszczak, J. V. *Solid State Commun.* **1985**, *56*, 1023.
(35) Ramanujachary, K. V.; Collins, B. T.; Greenblatt, M.; Waszczak, J. V. *Solid State Commun.* **1986**, *59*, 647.
(36) Ramanujachary, K. V.; Collins, B. T.; Greenblatt, M.; McNally, P.; McCarroll, W. H. *Solid State Ionics* **1986**, *22*, 105.
(37) Collins, B. T.; Ramanujachary, K. V.; Greenblatt, M.; McNally, P.; McCarroll, W. H. *J. Solid State Chem.*, to be submitted.
(38) Collins, B. T.; Ramanujachary, K. V.; Greenblatt, M. *J. Solid State Chem.*, to be submitted.
(39) Bither, T. A.; Gillson, J. L.; Young, H. S. *Inorg. Chem.* **1966**, *5*, 1559.
(40) Chamberland, B. L. *Inorg. Chem.* **1969**, *8*, 1183.
(41) Glemser, O.; Lutz, G. *Z. Anorg. Allg. Chem.* **1951**, *264*, 17.
(42) Wilhelmi, K.-A. *Acta Chem. Scand.* **1969**, *23*, 419.
(43) Glemser, O.; Hanschild, U.; Lutz, G. *Z. Anorg. Allg. Chem.* **1952**, *269*, 93.
(44) Glemser, O.; Lutz, G.; Meyer, G. *Z. Anorg. Allg. Chem.* **1956**, *285*, 173.
(45) Schollhorn, R.; Kuhlman, R.; Basenhard, J. O. *Mater. Res. Bull.* **1976**, *11*, 83.
(46) Birtill, J. J.; Dickens, P. G. *Mater. Res. Bull.* **1978**, *13*, 311.
(47) Dickens, P. G.; Birtill, J. J. *J. Electron Mater.* **1978**, *7*, 679.
(48) Dickens, P. G.; Birtill, J. J.; Wright, C. J. *J. Solid State Chem.* **1979**, *28*, 185.
(49) Dickens, P. G.; Pye, M. F. In *Intercalation Chemistry*; Whittingham, M. S., Jacobson, A. J., Eds.; Academic: New York, 1982; pp 539–559.
(50) Dickens, P. G.; Wiseman, P. J. In *International Review of Science, Inorganic Chemistry, Series II*; Roberts, L., Ed.; Butterworths: London, 1975; Vol. 10, p 211.
(51) Dickens, P. G.; Crouch-Baker, S.; Weller, M. T. *Solid State Ionics* **1986**, *18–19*, 89.
(52) (a) Goodenough, J. B. *Bull. Soc. Chim. Fr.* **1965**, 1200. (b) Goodenough, J. B. *Czech. J. Phys.* **1967**, *B17*, 304.
(53) Dickens, P. G.; Neild, D. J. *Trans. Faraday Soc.* **1968**, *64*, 13.
(54) Sperlich, G. *Z. Phys.* **1972**, *250*, 335.
(55) Joffe, V. A.; Patrina, I. V. *Sov. Phys.—Solid State* (*Engl. Transl.*) **1968**, *10*, 639.
(56) Goodenough, J. B. *Prog. Solid State Chem.* **1971**, *5*, 145.
(57) Whangbo, M. H.; Schneemeyer, L. F. *Inorg. Chem.* **1986**, *25*, 2424.
(58) Whangbo, M. H.; Canadell, E.; Schlenker, C. *J. Am. Chem. Soc.* **1987**, *109*, 6308.
(59) Graham, J.; Wadsley, A. D. *Acta Crystallogr.* **1966**, *20*, 93.
(60) Ghedira, M.; Chenavas, J.; Marezio, M.; Marcus, J. *J. Solid State Chem.* **1985**, *57*, 300.
(61) Zachariasen, W. H. *J. Less-Common Met.* **1978**, *62*, 1.
(62) Fogle, W.; Perlstein, J. *Phys. Rev. B: Condens. Matter* **1972**, *6*, 1402.
(63) Adler, D. *Solid State Phys.* **1968**, *21*, 1.
(64) (a) Kohn, W. *Phys. Rev. Lett.* **1967**, *19*, 439. (b) Halperin, B. I.; Rice, T. M. *Rev. Mod. Phys.* **1968**, 755. (c) *Solid State Phys.* **1968**, 116.
(65) Perloff, D. S. Ph.D. Thesis, Brown University, 1969, p 52.
(66) Travaglini, G.; Wachter, P.; Marcus, J.; Schlenker, C. *Solid State Commun.* **1981**, *37*, 599.
(67) Jandl, S.; Marcus, J.; Veuillen, J. Y., to be published.
(68) Band, G.; Sperlich, G. *Z. Phys.* **1975**, *B22*, 1.
(69) Bervas, E. Ph.D. Thesis, University of Grenoble, 1984.
(70) Travaglini, G.; Morke, I.; Wachter, P. *Solid State Commun.* **1983**, *45*, 289.
(71) Travaglini, G.; Wachter, P. In *Proceedings of the 15th Conference on the Physics of Semiconductors, Kyoto, 1980* (*J. Phys. Soc. Jpn., Suppl. A* **1980**, *49*, 869).
(72) Dierker, S. B.; Lyons, K. B.; Schneemeyer, L. F. *Bull. Phys. Soc.* **1984**, *29*, 469.
(73) Segransan, P.; Janossy, A.; Berthier, C.; Marcus, J.; Butaud, P. *Phys. Rev. Lett.* **1986**, *56*, 1854.
(74) Peierls, R. E. *Quantum Theory of Solids*; Clarendon: Oxford, 1955; p 108.
(75) Fröhlich, H. *Proc. R. Soc. London, A* **1954**, *A223*, 296.
(76) Gruner, G. *Perspectives in Solid State Physics*, to be published.
(77) (a) See, for example, the series: *Physics and Chemistry of Materials with Layered Structures*; Levy, F., Ed.; Vol. 2, 1976; Wieting, T. J., Schluter, M., Eds.; Vol. 3, 1979; Lee, P. A., Ed.; Vol. 4, 1976, Reidel: Dordrecht. (b) Toombs, G. A. *Phys. Rev. C:* **1978**, *40*, 181.
(78) Sato, M. *Lect. Notes Phys.* **1985**, *217*, 7.

(79) Sato, M.; Fujishita, H.; Hoshino, S. *J. Phys.* **1983**, *C16*, L877.
(80) Fleming, R. M.; Schneemeyer, L. F.; Moncton, D. E. *Phys. Rev. B: Condens. Matter* **1985**, *31*, 899.
(81) Pouget, J. P.; Moudden, A. H.; Moret, R.; Escribe-Filippini, C.; Hennion, B.; Marcus, J.; Schlenker, C. *Mol. Cryst. Liq. Cryst.* **1985**, *121*, 111.
(82) Butaud, P.; Segransan, P.; Berthier, C.; Dumas, J.; Schlenker, C. *Phys. Rev. Lett.* **1985**, *55*, 253.
(83) Nomura, K.; Kume, K.; Sato, M. *Solid State Commun.* **1986**, *57*, 611.
(84) Veuillen, J. Y.; Chevalier, R.; Salomon, D.; Dumas, J.; Marcus, J.; Schlenker, C. *Lect. Notes Phys.* **1985**, *217*, 129.
(85) Sato, M.; Fujishita, H.; Sato, S.; Hoshino, S. *Solid State Phys.* **1985**, *18*, 2603.
(86) Pouget, J. P.; Nguera, C.; Moudden, A. H.; Moret, T. *J. Phys.* **1985**, *46*, 1731.
(87) Sato, M.; Fujishita, H.; Hoshino, S. *J. Phys. C: Solid State Phys.* **1983**, *16*, L877.
(88) Wertheim, G. K.; Schneemeyer, L. F.; Buchanan, D. N. E. *Phys. Rev. B: Condens. Matter* **1985**, *32*, 3568.
(89) Dumas, J.; Schlenker, C.; Veuillen, J. Y.; Chevalier, R.; Marcus, J.; Cinti, R.; Al Khoury Nemeh, E. Proceedings, International Conference on Science and Technology of Synthetic Metals (ICMS 86), to be published.
(90) Johnston, D. C. *Phys. Rev. Lett.* **1984**, *52*, 2049.
(91) Schlenker, C. NATO–ASI on Low-Dimensional Conductors and Superconductors, Magog, Quebec, Canada, Aug 1986, to be published.
(92) Collins, B. T.; Ramanujachary, K. V.; Greenblatt, M., to be published.
(93) Dumas, J.; Schlenker, C.; Marcus, J.; Buder, R. *Phys. Rev. Lett.* **1983**, *59*, 757.
(94) See, for example: (a) Fleming, R. M. *Synth. Met.* **1986**, *13*, 241. (b) Fleming, R. M.; Cava, R. J.; Schneemeyer, L. F. *Physica B+C: (Amsterdam)* **1986**, *143B+C*, 95. (c) Fleming, R. M. NATO–ASI on Low-Dimensional Conductors and Superconductors, Magog, Quebec, Canada, Aug 1986, to be published.
(95) Mutka, H.; Boufard, S.; Dumas, J.; Schlenker, C. *J. Phys., Lett.* **1984**, *45*, L729.
(96) (a) Ong, N. P.; Verma, G.; Maki, K. *Phys. Rev. Lett.* **1984**, *52*, 663. Mazurkewich, G.; Gruner, G. *Phys. Rev. Lett.* **1983**, *51*, 2206. (b) Fleming, R. M.; Schneemeyer, L. F.; Cava, R. J. *Phys. Rev. B: Condens. Matter* **1985**, *31*, 1181.
(97) Cava, R. J.; Fleming, R. M.; Littlewood, P.; Rietman, E. A.; Schneemeyer, L. F.; Dunn, R. G. *Phys. Rev. B: Condens. Matter* **1984**, *30*, 3228.
(98) Dumas, J.; Schlenker, C.; Marcus, J.; Buder, R. *Phys. Rev. Lett.* **1983**, *50*, 757.
(99) Gill, J. C. *Solid State Commun.* **1981**, *39*, 1203.
(100) Fleming, R. M. *Solid State Commun.* **1982**, *43*, 167.
(101) Higgs, A. W.; Gill, J. C. *Phys. Rev. B: Condens. Matter* **1983**, *47*, 737.
(102) Fleming, R. M.; Schneemeyer, L. F. *Phys. Rev. B: Condens. Matter* **1983**, *28*, 6996.
(103) Mihaly, G.; Mihaly, L. *Phys. Rev. Lett.* **1984**, *52*, 109.
(104) Brill, J. W.; Herr, S. L. *Solid State Commun.* **1984**, *49*, 265.
(105) Kriza, G.; Mihaly, G. *Phys. Rev. Lett.* **1986**, *56*, 2529.
(106) Cava, R. J.; Fleming, R. M.; Rietman, E. A.; Dunn, R. G.; Schneemeyer, L. F. *Phys. Rev. Lett.* **1984**, *53*, 1677.
(107) Fleming, R. M.; Dunn, R. G.; Schneemeyer, L. F. *Phys. Rev. B: Condens. Matter* **1985**, *31*, 4099.
(108) Tamegai, T.; Tsutsumi, K.; Kagoshima, S.; Kanai, Y.; Tani, M.; Tomozowa, H.; Sato, M.; Tsuji, K.; Harada, J.; Sakata, M.; Nakajima, T. *Solid State Commun.* **1984**, *51*, 585.
(109) Tamegai, T.; Tsutsumi, K.; Kagoshima, S.; Kanai, Y.; Tomozawa, H.; Tani, M.; Nagami, Y.; Sato, M. *Solid State Commun.* **1985**, *56*, 13.
(110) Stephenson, N. C. *Acta Crystallogr.* **1966**, *20*, 59.
(111) Gatehouse, B. M.; Loyd, D. J. *Chem. Commun.* **1971**, 13.
(112) Gatehouse, B. M.; Loyd, D. J.; Miskin, B. K. *NBS Spec. Publ.* **1972**, *364*, 15.
(113) Vincent, H.; Ghedira, M.; Marcus, J.; Mercier, J.; Schlenker, C. J. *Solid State Chem.* **1983**, *47*, 113.
(114) (a) Kihlborg, L. *Ark. Kemi* **1963**, *21*, 471. (b) Kihlborg, L. **1963**, *21*, 365.
(115) Onoda, M.; Toriumi, K.; Matsuda, Y.; Sato, M. *J. Solid State Chem.* **1987**, *66*, 163.
(116) Onoda, M.; Matsuda, Y.; Sato, M. *J. Solid State Chem.* **1987**, *66*, 163.
(117) Ganne, M.; Dion, M.; Boumaza, A.; Tournoux, M. *Solid State Commun.* **1986**, *59*, 137.
(118) Shannon, R. D. *Acta Crystallogr., Sect. A* **1976**, *A32*, 751.
(119) Santoro, A.; Greenblatt, M.; McCarroll, W. H., unpublished data.
(120) Greenblatt, M.; McCarroll, W. H.; Niefeld, R.; Croft, M.; Waszczak, J. V. *Solid State Commun.* **1984**, *51*, 671.
(121) Greenblatt, M.; Ramanujachary, K. V.; McCarroll, W. H.; Niefeld, R.; Waszczak, J. V. *J. Solid State Chem.* **1985**, *59*, 149.
(122) (a) $T_c \sim 1.15$ K for an electrolytically grown crystal.[31] (b) Schlenker, C.; Schwenk, H.; Escribe-Filippini, C.; Marcus, J. *Physica B+C: (Amsterdam)* **1985**, *135*, 511.
(123) (a) Matsuda, Y.; Sato, M.; Onoda, M.; Nakao, K. *J. Phys. C: Solid State Phys.* **1986**, *19*, 6039. (b) Sato, M.; Matsuda, Y.; Fukuyama, H. *J. Phys. C: Solid State Phys.* **1987**, *20*, L137. (c) Ekino, T.; Akimitsu, J.; Matsuda, Y.; Sato, M. *Solid State Commun.* **1987**, *63*, 41.
(124) Dumas, J.; Escribe-Filippini, C.; Marcus, J.; Schlenker, C. Proceedings of the NATO DAVY Advanced Study Institute, Cambridge, U.K., 1983, Physics and Chemistry of Electrons and Ions in Condensed Matter.
(125) Dumas, J.; Bervas, E.; Marcus, J.; Salomon, D.; Schlenker, C.; Fillion, G. *J. Magn. Mater.* **1983**, *31–44*, 535.
(126) Escribe-Filippini, C.; Konate, K.; Marcus, J.; Schlenker, C.; Almairac, R.; Ayroles, R.; Roucau, C. *Philos. Mag. B:* **1984**, *50*, 321.
(127) Escribe-Filippini, C.; Marcus, J.; Schlenker, C.; Ayroles, R.; Roucau, C.; Kagoshima, S.; Pouget, J. P., to be published.
(128) DiSalvo, F. J.; Waszczak, J. V. *J. Phys. Chem. Solids* **1980**, *41*, 1311.
(129) Ramanujachary, K. V.; Greenblatt, M., to be published.
(130) Dumas, J.; Escribe-Filippini, C.; Marcus, J.; Mercier, J.; Salomon, D.; Schlenker, C.; Razavi, F. *Physica B: (Amsterdam)* **1983**, *117B*, *118B*, 602.
(131) Delaplace, R.; Molinie, P.; Jerome, D. *J. Phys., Lett.* **1976**, *37*, L13.
(132) Whangbo, M.; Canadell, E. *J. Am. Chem. Soc.*, in press.
(133) Stephenson, N. C.; Wadsley, A. D. *Acta Crystallogr.* **1965**, *19*, 241.
(134) Bang, G.; Sperlich, G. *Phys. Lett. A:* **1974**, *49*, 21.
(135) Sperlich, G. *J. Solid State Chem.* **1975**, *12*, 360.
(136) Travaglini, G.; Wachter, P.; Marcus, J.; Schlenker, C. *Solid State Commun.* **1982**, *42*, 407.
(137) Travaglini, G.; Wachter, P. *Solid State Commun.* **1983**, *47*, 217.
(138) Tsai, P. P.; Potenza, J. A.; Greenblatt, M.; Schugar, H. J. *J. Solid State Chem.* **1986**, *64*, 47.
(139) Brown, I. D. *Structure and Bonding in Crystals*; O'Keefe, M., Navrotsky, A., Eds.; Academic: New York, 1981; Vol. II, p 1.
(140) Ganne, M.; Dion, M.; Boumaza, A. *C.R. Seances Acad. Sci.* **1986**, *302*, 635.
(141) Tsai, P. P.; Potenza, J. A.; Greenblatt, M. *J. Solid State Chem.* **1987**, *69*, 329.
(142) Ramanujachary, K. V.; Greenblatt, M., to be published.
(143) Abrahams, S. C.; Marsh, P.; Schneemeyer, L. F.; Rice, C. E.; Spengler, S. E. *J. Mater. Res.* **1987**, *2*, 82.
(144) Kihlborg, L. *Ark. Kemi* **1963**, *21*, 357.
(145) Slade, R. C. T.; Halstead, T. K.; Dickens, P. G. *J. Solid State Chem.* **1980**, *34*, 1983.
(146) Schroder, F. A.; Weitzel, H. *Z. Anorg. Allg. Chem.* **1977**, *435*, 247.
(147) Tinet, D.; Canesson, P.; Estrade, H.; Fripiat, J. J. *J. Phys. Chem. Solids* **1979**, *41*, 583.
(148) Cirillo, A. C.; Ryan, L.; Gerstein, B. C.; Fripiat, J. J. *J. Chem. Phys.* **1980**, *73*, 3060.
(149) Shaver, P. J. *Appl. Phys. Lett.* **1967**, *11*, 255.
(150) Faughnan, B. W.; Crandall, R. S. In *Topics in Applied Physics*; Springer-Verlag: Berlin, 1980.
(151) Tinet, D.; Poncelet, G.; Fripiat, J. J. *J. Solid State Chem.*, to be published.
(152) (a) Marcq, P. J.; Poncelet, G.; Fripiat, J. *J. Catal.* **1984**, *87*, 339. (b) Sotani, N.; Yoshida, N.; Yoshioko, Y.; Kishimoto, S. *Bull. Chem. Soc. Jpn.* **1985**, *58*, 1626.
(153) (a) Sato, M.; Nakao, K.; Hoshino, S. *J. Phys. C: Solid State Phys.* **1984**, *17*, L817. (b) Sato, M.; Fujishita, H.; Sato, S.; Hoshino, S. *J. Phys. C: Solid State Phys.* **1986**, *19*, 3059.
(154) (a) Sato, M. Proceedings, International Conference on the Physics and Chemistry of Quasi-One-Dimensional Conductors, Lake Kawaguchi, Japan, 1986 (*Physica B+C: (Amsterdam)* **1986**, *143B+C*, 90). (b) Onoda, M.; Fujishita, H.; Matsuda, Y.; Sato, M. Proceedings, International Conference on Synthetic Metals, Kyoto, 1986. (c) Fujishita, H.; Shapiro, S. M.; Sato, M.; Hoshino, S. Proceedings, International Conference on the Physical and Chemical Properties of Quasi-One-Dimensional Conductors, Lake Kawaguchi, Japan, 1986 (*Physica B+C: (Amsterdam)* **1986**, *143B+C*, 201. (d) Fujishita, H.; Sato, M.; Sato, S.; Hoshino, S. *J. Solid State Chem.* **1987**, *66*, 40. (e) Sato, M.; Onoda, M.; Matsuda, Y. *J. Phys. C* **1987**, *20*, 4763.
(155) Kihlborg, L. *Acta Chem. Scand.* **1959**, *13*, 954.
(156) Ghedira, M.; Vincent, G.; Marezio, M.; Marcus, J.; Furcaudot, J. *J. Solid State Chem.* **1985**, *56*, 66.
(157) Magneli, A. *Acta Chem. Scand.* **1948**, *2*, 501.
(158) (a) Gruber, H.; Krantz, E.; Fritzer, H. P. *Phys. Status Solidi* **1981**, *65*, 589. (b) Gruber, H.; Haselmir, H.; Fritzer, H. P. *J. Solid State Chem.* **1983**, *47*, 84.

(159) (a) Guyot, H.; Schlenker, C.; Fourcadot, G. *Lect. Notes Phys.* **1985**, *217*, 133. (b) Guyot, H.; Schlenker, C.; Fourcaudot, G.; Konate, K. *Solid State Commun.* **1985**, *54*, 909. (c) Schlenker, C.; Parkin, S. S. P.; Guyot, H. *J. Magn. Magn. Mater.* **1986**, 54.
(160) Guyot, H.; Escribe-Filippini, C.; Fourcaudot, G.; Konate, K.; Schlenker, C. *J. Phys. C: Solid State Phys.* **1983**, *16*, L1227.
(161) Guyot, H.; Schlenker, C.; Pouget, J. P.; Ayroles, R.; Roucau, C. *J. Phys. C: Solid State Phys.* **1985**, *18*, 4427.
(162) McCarroll, W. H.; Darling, C.; Jakubicki, G. *J. Solid State Chem.* **1983**, *48*, 187.
(163) Moini, A.; Subramanian, M.; Clearfield, A.; DiSalvo, F. J.; McCarroll, W. H. *J. Solid State Chem.* **1987**, *66*, 136.
(164) Cox, D. E.; Cava, R. J.; McWhan, D. B.; Murphy, D. W. *J. Phys. Chem. Solids* **1982**, *43*, 657.
(165) Collins, B. T.; Greenblatt, M.; McCarroll, W. H. *J. Solid State Chem.*, in press.
(166) Whangbo, M.-H.; Canadell, E. *Inorg. Chem.* **1987**, *26*, 842.